Title

Replenishing IRAK-M expression in retinal pigment epithelium attenuates outer retinal degeneration

Authors

Jian Liu[1]*, David A. Copland[1], Alison J. Clare[1], Mathias Gorski[2], Burt T. Richards[3], Louis Scott[1], Sofia Theodoropoulou[1], Ursula Greferath[4], Katherine Cox[1], Gongyu Shi[1], Oliver H. Bell[1], Kepeng Ou[1], Jenna Le Brun Powell[5], Jiahui Wu[1], Luis Martinez Robles[6], Yingxin Li[5], Lindsay B. Nicholson[1,6], Peter J. Coffey[7], Erica L. Fletcher[4], Robyn Guymer[8], Monte J. Radeke[9], Iris M. Heid[2], Gregory S. Hageman[3], Ying Kai Chan[1,10], Andrew D. Dick[1,6,7,11]

Affiliations

[1]Academic Unit of Ophthalmology, Bristol Medical School, University of Bristol, Bristol BS8 1TD, United Kingdom.

[2]Department of Genetic Epidemiology, University of Regensburg, Regensburg 93053, Germany.

[3]Sharon Eccles Steele Center for Translational Medicine, John A. Moran Eye Center, University of Utah School of Medicine, Salt Lake City, UT 84132, United States.

[4]Department of Anatomy and Physiology, University of Melbourne, Melbourne, 3010 VIC, Australia.

[5]Translational Health Sciences, Bristol Medical School, University of Bristol, Bristol BS8 1TD, United Kingdom.

[6]School of Cellular and Molecular Medicine, University of Bristol, Bristol BS8 1TD, United Kingdom.

[7]Institute of Ophthalmology, University College London, London EC1V 9EL, United Kingdom.

[8]Centre for Eye Research Australia, Royal Victorian Eye and Ear Hospital, University of Melbourne, Melbourne, 3010 VIC, Australia.

[9]Neuroscience Research Institute, University of California, Santa Barbara, CA 93106, United States.

[10]Wyss Institute for Biologically Inspired Engineering, Harvard University, Boston, MA 02215, United States.

[11]National Institute for Health Research Biomedical Research Centre, Moorfields Eye Hospital, London EC1V 2PD, United Kingdom.

*Corresponding author: Jian Liu, jian.liu@bristol.ac.uk

OVERLINE: RETINAL DISEASE

One-Sentence Summary: IRAK-M protects the retinal pigment epithelium and is a potential therapeutic target for macular degeneration

Abstract

Chronic inflammation is a constitutive component of many age-related diseases, including age-related macular degeneration (AMD). Here, we identified interleukin-1 receptor-associated kinase (IRAK)-M as a key immunoregulator in retinal pigment epithelium (RPE) that declines during the aging process. Rare genetic variants of *IRAK3*, which encodes IRAK-M, were associated with an increased likelihood of developing AMD. In human samples and in mouse models, IRAK-M abundance in the RPE declined with advancing age or exposure to oxidative stress and was further reduced in AMD. *Irak3*-knockout mice exhibited an increased incidence of outer retinal degeneration at earlier ages, which was further exacerbated by oxidative stressors. The absence of IRAK-M led to a disruption in RPE cell homeostasis, characterized by compromised mitochondrial function, cellular senescence, and aberrant cytokine production. IRAK-M overexpression protected RPE cells against oxidative or immune stressors. Subretinal delivery of adeno-associated virus (AAV) expressing human *IRAK3* rescued light-induced outer retinal degeneration in wild-type mice and attenuated age-related spontaneous retinal degeneration in *Irak3*-knockout mice. Our data support that replenishment of IRAK-M in the RPE may redress dysregulated pro-inflammatory processes in AMD, suggesting a potential treatment for retinal degeneration.

Main Text

INTRODUCTION

Cell-autonomous responses, such as metabolic regulation, autophagy and immune-mediated inflammation, initiated by environmental stressors are active processes that help to maintain homeostasis (*1*). However, loss of immune regulation and persistent inflammation can lead to acute or chronic tissue damage. Chronic inflammation, accentuated by aging (inflammaging), is implicated in progression of many age-related degenerative disorders (*2*).

The retinal pigment epithelium (RPE) is essential for maintaining outer retinal function and ocular immune privilege. RPE dysfunction results in photoreceptor (PR) loss and gradual decline of the central visual acuity, as observed in age-related macular degeneration (AMD) (*3-5*). AMD, a progressive, multifactorial disease, is a leading cause of irreversible severe vision loss among the elderly. Alongside aging, the interplay of oxidative stress and chronic inflammation, fueled by genotype-predisposed susceptibility and environmental stressors, contributes significantly to AMD pathogenesis. Genome-wide association studies have identified risk loci for AMD, including genes in the complement pathway and *age-related maculopathy susceptibility 2* (*ARMS2*)/*HtrA serine peptidase 1* (*HTRA1*) alleles (*6, 7*). Rare coding variants in complement regulatory genes such as complement factor H (*CFH*) and complement factor I (*CFI*) have been associated with AMD risk, leading to the development of complement inhibitors and gene therapies (*8, 9*). AMD pathogenesis involves multiple pathways, including oxidative stress and innate immune responses (*10, 11*). In mice, for example, a high-fat diet is required to initiate pathology on the background of complement gene mutation (*12*). Therefore, elucidating the factors central to the diverse pathologies in AMD is critical, irrespective of genetic risk.

Several inflammatory pathways are associated with AMD progression, including activation of the complement cascade, NLRP3 (nucleotide-binding domain, leucine-rich–containing family, pyrin domain–containing-3) inflammasome, production of cytokines and chemokines, immune cell

infiltration, and immune activation of retinal microglia and RPE (*13-17*). Toll-like receptors (TLRs), particularly TLR2, 3 and 4, are implicated in AMD development (*18-20*). The Myddosome, an oligomeric complex consisting of myeloid differentiation primary response 88 (MyD88) and interleukin (IL)-1 receptor (IL-1R)-associated kinase (IRAK) family proteins, is essential for transmitting TLR and inflammasome-IL-1R axis-mediated signals (*16*). Myddosome signaling also promotes inflammasome activation (*21*). Although Myddosome overactivation has been observed in RPE from patients with geographic atrophy (late-stage atrophic AMD) (*16*), questions remain regarding its role in AMD progression and the specific Myddosome components driving TLR/IL-1R pro-inflammatory signaling dysregulation.

The RPE exhibits a high number of differentially expressed genes (DEGs) overlapping with those associated with aging and age-related retinal diseases (*22*). Disturbances in RPE intracellular processes, such as autophagy and senescence, compounded by oxidative stress, lead to inflammasome activation and IL-1β/IL-18 release (*17, 23, 24*). The magnitude of oxidative stress-induced inflammation is largely determined by various TLRs and balanced by counteracting mechanisms regulated by inhibitors including IRAK-M (encoded by *IRAK3*) (*25, 26*). IRAK-M is a pseudokinase that downregulates the pro-inflammatory cascade by impeding phospho-IRAK1/4 uncoupling from the Myddosome for transforming growth factor (TGF)-β-activated kinase 1 (TAK1)-dependent nuclear factor (NF)-κB activation, or by inducing downstream anti-inflammatory responses through the IRAK-M/MyD88 complex and IRAK-M/MEKK3 (mitogen activated protein kinase kinase kinase 3) pathway (*27, 28*).

IRAK-M expression is regulated by both epigenetic and transcriptional mechanisms, in response to numerous endogenous and exogenous factors including IL-1β, TGF-β1, granulocyte-macrophage colony-stimulating factor (GM-CSF), and adiponectin, as well as cell surface receptors or intracellular molecules including TLRs, triggering receptor expressed on myeloid cells 1 (TREM-1) and phosphoinositide 3-kinase (PI3K) (*29, 30*). Downregulation of IRAK-M

signaling is associated with exaggerated oxidative stress and systemic inflammation in metabolic disorders such as insulin resistance and obesity (*31*). Reduced *IRAK3* mRNA expression in monocytes and adipose tissues of obese patients leads to elevated mitochondrial stress, systemic inflammation, and metabolic syndrome (*31*). Multiple mutations in *IRAK3* have been associated with early-onset chronic asthma in humans (*32*).

Given *IRAK3* expression in RPE cells in vitro (*23*), we hypothesized its potential regulatory relevance in retinal aging and degeneration. The present study aimed to elucidate the role of IRAK-M in AMD by assessing genetic variants and their association with AMD risk. We also evaluated IRAK-M expression in patient samples and mouse models of retinal degeneration, alongside alterations in retinal function in *Irak3*-knockout (KO) mice. Furthermore, we explored the therapeutic potential of IRAK-M augmentation in protecting RPE and outer retina against degenerative processes in murine models.

RESULTS

Rare protein-altering variants of *IRAK3* are associated with increased risk of late AMD

In view of the observation of Myddosome activation in AMD (*16*), we asked whether variants in the genes encoding Myddosome components contribute to disease risk and pathogenic pathways. Single variant analyses have limited power to depict rare variants with association. Gene-based burden tests, which assess accumulated association from multiple rare variants per gene, complement such analyses and enhance the ability to detect a disease burden. As such, we applied burden tests of the genetic data from the International AMD Genomics Consortium (IAMDGC) that contains 16,144 late AMD cases versus 17,832 age-matched controls (*6*). The analysis revealed no association between rare variants of *MYD88* and late AMD ($P = 0.95$). We then examined the cumulative effect of rare protein-altering variants for the IRAK family kinases

(*IRAK1-4*), which revealed a statistically significant late AMD risk-increasing signal for *IRAK3* (P = 0.012) (Table 1). Table S1 lists the variants in the *IRAK3* gene region, including 18 polymorphic variants that were detected in both AMD cases and controls and used in the gene burden test. As a comparator for *IRAK3*, rare variants of *IL33*, which encodes a Th2-oriented cytokine linked to retinal pathophysiology *(33-35),* were not associated with late AMD (P = 0.18).

IRAK-M expression in the RPE is reduced with age and to a greater extent in AMD patients

We next explored IRAK-M expression in the retina by performing immunohistochemistry on human retinal cryosections from a young-age normal eye (age and gender details reported in Table S2). We found abundant IRAK-M distribution at the RPE layer, with faint or subtle immunopositivity observed in other retinal layers, including GCL (ganglion cell layer), IPL (inner plexiform layer), OPL (outer plexiform layer), ONL (outer nuclear layer), POS (PR outer segment), and choroid (Fig. 1A and B). Immunohistochemistry of a second donor eye also demonstrated IRAK-M expression in RPE and choroid in sections from an old-age normal eye (Table S2, fig. S1, A and B). IRAK-M was detected in mouse RPE (fig. S1, C to E), consistent with our previously reported detection of *Irak3* transcript in a murine RPE cell line (*23*). We observed strong immunopositivity of IRAK-M in both inner (non-pigmented) and outer (pigmented) ciliary epithelium of human eyes (fig. S1, F and G), suggesting a potential regulatory role in barrier cells.

We next determined whether the abundance of IRAK-M altered during aging. Total RNA was harvested from 6-mm trephine tissue punches of 227 extramacular and 159 macular RPE/choroids, as well as 238 extramacular and 242 macular retinas. Total RNA yield and RNA integrity number (RIN) scores were measured to confirm the consistency of the quality of RNA samples across the age (fig. S2, A and B). Microarray analysis of these samples - identified an age-dependent decrease in *IRAK3* expression in the macular (R^2=0.0408, P=0.0104; Fig. 1C) and extramacular (R^2=0.0403,

P=0.0025; fig. S2C) RPE/choroid but no change in expression in the retina (Fig. 1C and fig. S2D). Neither *IRAK1* nor *IRAK4* expression changed with age in RPE/choroid or retina (Fig. 1C and fig. S2, C and D). Further analyses of IRAK-M protein abundance in sex-mixed human RPE/choroid lysates across a range of age groups (Table S2) revealed significant reduction in samples from elderly individuals (76-84y) compared to young (20-22y, P = 0.004) or middle-aged (52-59y, P = 0.041) samples (Fig. 1D). Increased abundances of phospho-IRAK4 and phosphor-NF-κB p65 were also detected (fig. S3A), suggesting activation of inflammatory signaling pathways. CFH and C3 protein abundance did not change with age (fig. S3A). As with human samples, RPE isolated from aged mice (19-24m) had lower IRAK-M protein abundance compared with younger mice (2-5m, fig. S3B). The abundance of IRAK-M protein in mouse retinal $CD11b^+$ cells (MACS-isolated-microglia and perivascular macrophages) was also reduced with age (fig. S3C).

To ascertain whether *IRAK3* expression was compromised in AMD, as compared to age-matched controls, we analyzed a published RNA-seq dataset (GSE99248), which included PORT-normalized counts for both sense and antisense transcripts (*36*). In the *IRAK* family genes, only *IRAK3* mRNA in RPE/choroid/sclera, and not in the retina, was lower in AMD than age-matched controls (Fig. 2A). *IRAK1*, *IRAK2* and *IRAK4* expression, as well as antisense RNAs specific to any *IRAK*, were unchanged between AMD and controls (Fig. 2A). From the same dataset, we also examined the expression of other known genes for negative regulation of TLR/IL-1R/MyD88/IRAK1/4 signaling (fig. S4), including *PIN1* (peptidylprolyl cis/trans isomerase, NIMA-interacting 1, which inhibits TLR transcription factor IRF3), *IL1RN* (IL-1R antagonist), *SOCS1* (suppressor of cytokine signaling 1, which induces MAL ubiquitination required for MyD88 activation), *TOLLIP* (Toll-interacting protein, which binds to IRAK1 to induce translocation of TLRs to endosome for degradation), *FADD* (Fas-associated death domain, which interacts with IRAK1/MyD88 to attenuate the signaling), and *PTPN6* (Tyrosine-protein phosphatase non-receptor type 6, which inhibits SYK activation and blocks MyD88

phosphorylation). None of these genes showed any significant difference between AMD and controls ($P > 0.05$, fig. S4).

To further determine the spatial expression of IRAK-M protein within tissue associated with age and AMD, we performed IHC on paraffin-embedded retinal sections of 2 'young' (30 and 59y-old) and 5 'aged' (76-97y) individuals without recorded ocular diseases, and 11 AMD patients (76-95y). Table S2 contains detailed age and sex information for these samples. The paraffin slides were visualized using alkaline phosphatase-based IHC due to strong autofluorescence of the RPE that was not fully blocked by Sudan black B quenching. IRAK-M (stained in red) was observed in multiple layers of the retina, RPE and choroid (Non-AMD 59y, Fig. 2B and fig. S5A). In aged control and AMD samples, the pattern and strength of IRAK-M-immunopositive signals was variable, for example with a heightened signal in OPL/ONL (Non-AMD 97y, Fig. 2B and fig. S5B), in INL/ONL/IS (inner segment) (Mild AMD 76y, Fig. 2B and fig. S5C), or in NFL (nerve fiber layer) (Unidentified stage AMD 85y, Fig. 2B and fig. S5D). Furthermore, we observed an intensified Bruch's membrane (BM) in retinal sections of AMD patients (Fig. 2B), which was not seen in non-AMD samples (*37*). After color deconvolution using the Fiji package of ImageJ, IRAK-M signal (red) and RPE pigment (brown) were separated for quantification. IRAK-M expression was lower in AMD-macular RPE compared to age-matched non-AMD-macular RPE (Fig. 2C). In macular areas of choroid or retina, despite a trend of reduction in AMD, the difference in IRAK-M expression between AMD and age-matched non-AMD was not statistically significant ($P > 0.05$, Fig. 2C). In extramacular tissues, IRAK-M expression in RPE, choroid or retina did not significantly differ between AMD and non-AMD samples ($P > 0.05$, Fig. S6).

Irak3-KO mice acquire earlier outer retinal degeneration during aging

We then investigated whether aging and lack of *Irak3* affected outer retinal degeneration in *Irak3*-KO mice (*Rd8* mutation removed, as confirmed in fig. S7A). In this strain, the exons 9-11 of *Irak3*

were removed by homologous recombination, resulting in a mutant IRAK-M protein missing two-thirds of the pseudokinase domain (*38, 39*). The multiple conserved cysteine residues within the dimeric structure of the pseudokinase domain of native IRAK-M are essential in forming an interactive interface with IRAK4 for the negative regulation of IRAK-Myddosome signaling (*40*). Pathological changes in the retina were tracked for 15 months using fundoscopy and optical coherence tomography (OCT). Repeated imaging of the same affected retinas unveiled the emergence of white spots with aging (Fig. 3A), along with an increase in the number of retinas displaying varying counts of fundus white spots in *Irak3*-KO mice, elevating from 5 out of 22 eyes at 2 months to 15 out of 30 eyes at 5 months (Fig. 3A and B, and fig. S7B). Fundus white spots in mice have been well described as a feature of foci of inflammation linked to accumulated macrophages/microglia in the outer retina and subretinal space, where they phagocytose damaged photoreceptors and RPE (*41-45*). The incidence of abnormal retinal appearance reached 21 out of 26 by 15m (Fig. 3B). In comparison, there was no progression of white spots in the retinas of WT mice to 12m; however WT retinas displaying white spots markedly increased as mice aged, with16 out of 26 retinas displaying white spots by 19-21m (Fig. 3B). These data suggest accelerated aging-associated retinal abnormalities and degeneration associated with *Irak3* mutation. We also noted that the early appearance of retinal white spots in *Irak3*-KO mice was accompanied by outer retinal lesions identified by OCT (Fig. 3C).

Given the link between fundus spots and microglia/macrophage activation in various murine models of retinal degeneration (*41-45*), we evaluated the $CD11b^+$ myeloid cell populations in the murine retina. As expected, increased numbers of $CD11b^+$ cells in the ONL (fig. S7C) and $CD11b^+$ cell accumulation in the subretinal space (fig. S7D) were observed in $Irak3^{-/-}$ mice, associated with increased number of TUNEL-positive RPE cells in multiple focal areas on the surface of RPE/choroidal flatmounts (Fig. 3D). Although no difference in retinal thickness was found at 5m between WT and $Irak3^{-/-}$ mice, the outer retina layers (ORL, see Supplementary Methods for

254 definition) of *Irak3*$^{-/-}$ mice was thinner by 12-13m (Fig. 3E). By 12m there were significant
255 increases ($P < 0.05$) in *Ccl2* (*chemokine C-C motif ligand 2*) and *Il1b* mRNA expression
256 (normalized to *RPS29*) in *Irak3*$^{-/-}$ RPE/choroid compared to WT counterparts (Fig. 3F), suggesting
257 a pro-inflammatory tissue environment. The relative mRNA expression of cytokines in the retina
258 were all below 0.005 regardless of genotypes - much lower than those in RPE/choroid – although
259 *Il12* expression was upregulated in *Irak3*$^{-/-}$ retina (Fig. 3F). We were unable to compare tissue
260 cytokine protein concentrations due to undetectability or trace amounts of the cytokines in
261 RPE/choroid and retina samples. Systemically, concentrations of serum cytokines, including
262 tumor necrosis factor (TNF)-α, monocyte chemoattractant protein (MCP)-1 and IL-10, in *Irak3*$^{-/-}$
263 mice were significantly higher than those in WT mice ($P < 0.05$, fig. S7E).
264
265 **Oxidative stress reduces RPE IRAK-M abundance, and loss of IRAK-M increases**
266 **susceptibility of outer retinal layers to oxidative damage**
267 Age-associated accumulation of oxidative stress in the RPE is a recognised contributor to the
268 progression of AMD. To examine if oxidative stress could be an independent factor for the
269 reduction of IRAK-M, we applied oxidative stressors both in vitro and in vivo.
270 In vitro, we examined early passage (<8) human retinal pigment epithelial ARPE-19 cells to reduce
271 variability. Confluent ARPE-19 cells exhibited RPE features, including cobblestone-like
272 morphology, and expressed tight junction protein zonula occludens-1 (ZO-1) and RPE-specific
273 protein RPE65 (fig. S8A). ARPE-19 cells were treated with different doses of paraquat) for up to
274 72h to induce mitochondrial ROS, which caused dose-dependent cytotoxicity as assessed by a
275 lactate dehydrogenase (LDH) cytotoxicity assay (fig. S8B). IRAK-M abundance was suppressed
276 by 72h exposure to a sub-toxic dose of paraquat (0.25mM) (fig. S8C). Reduction in IRAK-M was
277 accompanied by increased secretion of pro-inflammatory cytokines HMGB1 (high mobility group
278 box 1), IL-18 and GM-CSF, and decreased secretion of anti-inflammatory IL-11 (fig. S8D).

Crucially, downregulation of IRAK-M also occurred in human induced pluripotent stem cell (iPSC)-derived RPE cells following 72h treatment of sub-toxic doses of paraquat (0.25-0.5mM) (fig. S8, E and F).

In vivo, retinal oxidative damage was introduced by fundus camera-directed light exposure (100kLux for 20min) (*46*) or intravitreal administration of paraquat (2µl at 1.5mM) (*47*) in C57BL/6J WT mice aged 8w. Western blot analyses showed that IRAK-M abundance in the RPE lysate was abated after 7 days in both models (Fig. 4, A and B). In separate experiments, fundoscopy and OCT images obtained on day 14 displayed the fundal appearance of white spots (red arrows, Fig. 4C and D), alongside thinning of the outer retina in the light-induced retinal degeneration (LIRD) model (Fig. 4E), as well as reduced thickness in outer and a partial decrease in inner retinal thickness in the paraquat model (Fig. 4F). Retinal oxidative stress was then induced in adult WT and *Irak3* $^{-/-}$ mice (8w old) by light induction. *Irak3*$^{-/-}$ mice exhibited greater thinning of the retina following light challenge, particularly the ORL (Fig. 4G).

AP-1 regulates IRAK-M expression in RPE cells in age-dependent manner

Known transcription factors regulating IRAK-M expression in monocytes or lung epithelial cells include AP-1 and C/EBP-β (*29, 48*). We found that, in addition to an age-associated reduction in IRAK-M abundance (Fig. 1D), abundance of c-Jun, an AP-1 subunit, was decreased in aged samples compared to young controls (fig. S9, A and B). c-Fos, another AP-1 subunit, was also reduced in old age compared to middle-age samples , whereas there was no change in C/EBP-β abundance between samples (fig. S9, A and B).

The binding of c-Jun and c-Fos to the IRAK-M promoter region was confirmed by chromatin immunoprecipitation (ChIP) assay on ARPE-19 cells, and this was increased by lipopolysaccharide (LPS) stimulation for 24h (fig. S9C). ARPE-19 cells treated with paraquat for 72h showed decreased phosphorylation of both c-Jun and c-Fos, and total c-Jun and c-Fos were

downregulated by higher dose of paraquat only (fig. S9D). The JNK inhibitor SP600125 or the c-Fos/AP-1 inhibitor T5224 at 20 μM also decreased IRAK-M abundance in ARPE-19 cells (fig. S9D). Consequently, treatment with SP600125 or T5224 resulted in enhanced ARPE-19 susceptibility to paraquat-induced cytotoxicity (fig. S9E), as did *IRAK3* siRNA (fig. S9F).

IRAK-M deficiency induces RPE mitochondrial dysfunction and senescent phenotype which is protected by IRAK-M augmentation

To elucidate metabolic mechanisms involved in IRAK-M deficiency-induced retinal degeneration, we examined RPE cell metabolism and senescence using primary mouse RPE cells. The RPE cells from *Irak3*$^{-/-}$ mice showed reduced basal mitochondrial respiration (BR) and adenosine triphosphate (ATP) production compared to WT (fig. S10A), whereas no differences in basal glycolysis (BG) and maximal glycolytic capacity (MGC) were observed between genotypes (fig. S10B). These data suggest a role for IRAK-M in the maintenance of mitochondrial function in RPE cells. *Irak3* $^{-/-}$ RPE cells were more prone to oxidative stressor (paraquat or H_2O_2)-induced senescent phenotype, with increased activity of senescence-associated β-galactosidase (SA-β-gal, fig. S10C), increased abundance of cyclin-dependent kinase inhibitor $p21^{CIP1}$ and decreased nuclear lamin B1 (LB1, fig. S10D), and increased secretion of IL-6 (a senescence-associated cytokine) (*17*) (fig. S10E). The basal secretion of the pro-inflammatory cytokine HMGB1 of *Irak3*$^{-/-}$ RPE cells was higher than the WT cells, while secretion in response to oxidative stressors was comparable (fig. S10F).

We then examined whether overexpression of endogenous IRAK-M protein could protect RPE via CRISPR/Cas9 (clustered regularly interspaced short palindromic repeats and CRISPR-associated protein 9)-mediated gene expression. Following the augmentation of IRAK-M abundance in human iPSC-derived RPE cells confirmed by Western blot (fig. S11A), the cells were treated with either H_2O_2 or LPS. Oxygen consumption rate analysis demonstrated that basal and maximal

mitochondrial respiration were both sustained by IRAK-M overexpression, but impaired in sham-transfected cells following oxidative or immune stresses (Fig. 5A). Although untreated IRAK-M-overexpressing iPSC-RPE cells displayed lower maximal glycolytic activity than control plasmid-transfected cells, glycolytic activity remained stable upon H_2O_2 or LPS treatment, whereas glycolytic activity in control cells was reduced by 24h treatment with H_2O_2 or LPS (Fig. 5B). The lower glycolytic activity in un-stressed iPSC-RPE with overexpressed IRAK-M may indicate lower bio-energetic dependency on glucose, suggesting possible benefits to glucose-dependent photoreceptors (*49*).

Overexpression of IRAK-M in ARPE-19 cells promoted the formation of autophagosomes [light chain 3B (LC3B)-green fluorescent protein (GFP)] and autolysosomes [LC3B-red fluorescent protein (RFP)] following H_2O_2 or LPS treatment, suggesting an upregulated autophagy flux (fig. S11, B and C). Moreover, IRAK-M overexpression in ARPE-19 cells ameliorated the SA-β-gal activity and HMGB1 secretion induced by sub-toxic doses of paraquat (0.25 mM) (fig. S11, D and E), and reduced the LDH release induced by a toxic dose of paraquat (1 mM) (fig. S11F).

We created stably transfected RPE cell lines maintained in selective medium from a parent mouse B6-RPE07 cell line that expressed either mouse *Irak3* or human *IRAK3* mRNA, as evidenced by quantitative RT-PCR (fig. S12A). Expression of mouse *Irak1* and *Irak4* were not affected. Human *IRAK3*-expressing mouse cells showed a decrease in DNA binding activity of nuclear NF-κB after LPS stimulation (fig. S12B), supporting that transduced human *IRAK3* is as functional as its murine counterpart in suppressing NF-κB activation in mouse RPE. Stably transfected RPE cells overexpressing human *IRAK3* experienced less cytotoxicity than sham-transfected cells after four days of confluency (Fig. 5C) and exhibited a reduced stressor-induced cytotoxicity after treatment with paraquat (0.125 mM) or LPS (40 ng/ml) for 3 days (Fig. 5D). To exclude the possible contribution of native mouse *Irak3* to cell response observed, we performed transient transfection on primary RPE cells isolated from *Irak3*$^{-/-}$ mice. Similar to data from human iPSC-RPE cells

using CRISPR/Cas9 activation plasmid (Fig. 5A and B), maximal mitochondrial respiration was retained in mouse primary *Irak3*$^{-/-}$ RPE cells transduced with human *IRAK3* after 24h H_2O_2 treatment (Fig. 5E). H_2O_2 -induced oxidative stress had no effect on glycolysis in *Irak3*$^{-/-}$ RPE cells, regardless of human *IRAK3* transduction (Fig. 5F).

AAV2.Cytomegalovirus (CMV) promoter-mediated human *IRAK3* expression suppresses light-induced retinal degeneration in wild-type mice

To date, AAV2 is the best clinically validated AAV serotype to treat RPE-related retinal pathologies when administrated subretinally and leads to durable gene expression and efficacy without inducing deleterious immune activation (*50*). In non-human primates (NHPs) and mice, subretinal injection of AAV2.CMV preferably transduces the RPE, and, at higher doses, photoreceptors (*51, 52*).

We therefore administered AAV2.CMV subretinally to introduce human *IRAK3* expression in C57BL/6J mice. To identify the dose-dependent transduction efficacy, 2 µl of AAV2 encoding enhanced GFP (EGFP) under the control of the constitutive CMV promoter (AAV2.CMV.EGFP) at 1×10^{12} or 2×10^{11} gc/ml were subretinally delivered into mouse eyes. The 'high dose' (1×10^{12} gc/ml in 2 µl, or 2×10^{9} gc/eye) induced more pronounced EGFP expression 2-11 weeks after injection than the "low dose" (2×10^{11} gc/ml or 4×10^{8} gc/eye) (fig. S13). Administration with AAV2.CMV.h*IRAK3* induced a dose-dependent human *IRAK3* mRNA expression in RPE/choroid two weeks after injection, compared to a similar vector but with no transgene used as a control 'null' vector (Fig. 6A). Low mRNA expression of exogenous human *IRAK3* was detected in the retina, at levels 17.1-fold lower than that in the RPE/choroid (Fig. 6A). Using an antibody specific to human IRAK-M protein, we confirmed that the exogenous IRAK-M was largely expressed in the RPE by immunohistochemistry (Fig. 6B).

To evaluate the protective effects of *IRAK3* transgene expression in vivo, we applied LIRD in mice 2 weeks after AAV injection (2×10^9 gc/eye). Light exposure of the null AAV2-injected eyes resulted in a decrease of outer retinal thickness, whereas AAV2.CMV.h*IRAK3* treatment reduced light-induced outer retinal thinning two weeks after light exposure (Fig. 6C). TUNEL staining in the ONL was also reduced by AAV2.CMV.h*IRAK3* (Fig. 6D). Mitochondrial staining in the IS was improved in LIRD mice treated with AAV2.CMV.h*IRAK3* compared to null AAV2-injected mice (Fig. 6E). The differences of mitochondrial staining in the GCL, IPL and OPL between control and LIRD mice were not significant ($P > 0.05$), irrespective of AAV2.CMV.h*IRAK3* treatment (Fig. 6E).

RPE-specific *IRAK3* expression attenuates light-induced RPE and outer retinal degeneration in wild-type mice

We next utilized the RPE-specific Bestrophin-1 (Best1) promoter to elucidate whether AAV2-mediated overexpression of *IRAK3* exclusively in the RPE also conferred protection. In line with previous data showing the superiority of CMV promoter over Best1 promoter in driving transgene expression in mouse RPE (*53, 54*), we found that AAV2.Best1 required a higher multiplicity of infection (MOI 100,000) to ensure comparable expression of human *IRAK3* mRNA in mouse B6-RPE07 cells than AAV2.CMV (MOI 50,000) (fig. S14). Similarly, a two times higher AAV2.Best1 vector dose (4×10^9 gc/eye) than AAV2.CMV (2×10^9 gc/eye) was needed to give robust expression of human IRAK-M protein in the RPE of mice (Fig. 7A). We therefore used AAV2.Best1.h*IRAK3* at 4×10^9 gc/eye and AAV2.CMV.h*IRAK3* at 2×10^9 gc/eye for subsequent treatments.

To evaluate therapeutic effects of *IRAK3* gene therapy under a more severe experimental setting, we augmented outer retinal damage using a fluorescein (FL)-assisted LIRD model that renders the retina more susceptible to light exposure (*46, 55*). Three weeks after subretinal delivery of

AAV2.CMV.h*IRAK3* (2×10^9 gc/eye), AAV2.Best1.h*IRAK3* (4×10^9 gc/eye), or AAV2.CMV.Null (2×10^9 or 4×10^9 gc/eye), WT mice were subjected to the FL-assisted light injury (*46*). Two weeks after light exposure, while the FL-assisted approach in null vector-injected control eyes caused a reduction in ORL thickness by 43.9%, both AAV2.CMV.h*IRAK3* and AAV2.Best1.h*IRAK3* reduced the degree of ORL thinning (Fig. 7B). Whole RPE flatmounts were stained with antibodies recognizing a tight junction-associated protein (ZO-1) and a mitochondrial marker (translocase of outer mitochondrial membrane 20, Tom20). Three representative areas 0.4 mm distant to the optic nerve head of each flatmount were imaged. Light exposure induced RPE disorganization and mitochondrial damage, demonstrated by appearance of enlarged cells, disarray of hexagonal morphology, and loss of staining for ZO-1 and Tom20 (Fig. 7C). AAV2.CMV.h*IRAK3* and AAV2.Best1.h*IRAK3*, each resulted in amelioration of RPE morphological abnormalities and preservation of ZO-1 and Tom20 staining. Tom20 staining was more pronounced adjacent to the cell membrane of RPE cells (Fig. 7C), suggesting mitochondrial mobilization towards the intercellular junction sites (*56*).

AAV2.CMV-mediated *IRAK3* expression suppresses spontaneous outer retinal degeneration in *Irak3*$^{-/-}$ mice

We then investigated whether AAV-*IRAK3* could attenuate outer retinal degeneration caused by *Irak3* knockout and aging. We administered AAV2.CMV.h*IRAK3* or AAV2.CMV.Null (2×10^9 gc/eye) subretinally in young *Irak3*$^{-/-}$ mice (2-4m old) and allowed them to age. Six months after subretinal delivery of AAV vectors, AAV2.CMV.h*IRAK3* blunted the age-dependent occurrence of retinal spots (Fig. 8, A and B) and reduced the number of retinal spots in *Irak3*$^{-/-}$ mice compared to AAV2.CMV.Null (8-10m old; Fig. 8C). The effect was more pronounced within the treatment side of the retina receiving the vector, as expected (Fig. 8C). Compared to AAV2.CMV.Null-

427 treated mice, mice receiving AAV2.CMV.h*IRAK3* experienced less outer retinal thinning at
428 0.2mm from the optic nerve head (Fig. 8D).
429
430
431 **DISCUSSION**
432 Here, we have demonstrated a protective role for the immune regulator IRAK-M in the metabolic
433 and immune homeostasis of the RPE. A feed-forward loop with aging, oxidative stress and decline
434 in abundance of IRAK-M may generate a pro-inflammatory microenvironment driving retinal
435 degeneration. We have shown that replenishing IRAK-M can maintain mitochondrial function,
436 inhibit senescence and promote cell survival, protecting the retina from degeneration in a LIRD
437 mouse model and in *Irak3*$^{-/-}$ mice. Because IRAK-M is reduced with aging, oxidative stress and
438 AMD, the replenishment of IRAK-M may be a therapeutic strategy for treating AMD patients.
439 Previous research has demonstrated expression of IRAK-M in cells other than
440 monocytes/macrophages, including airway and intestine epithelium, fibroblasts, neurons,
441 neutrophils, dendritic cells basophils and B cells (*39, 57, 58*). Mutant *IRAK3* has been link to
442 asthma (*32*). Tarallo *et al.* reported aberrant activation of NLRP3-inflammasome and Myddosome
443 signaling, such as increased phospho-IRAK1/4 expression in RPE lysates of patients with
444 geographic atrophy, but did not probe IRAK-M (*16*). Here we found that the abundance of IRAK-
445 M declines with age in the RPE but not retinal tissue and is reduced further in patients with AMD
446 compared to age-matched controls. Furthermore, IRAK-M was expressed by bilayer ciliary
447 epithelium, suggesting distribution in other ocular epithelium barriers. The RPE regulates and
448 protects against excessive oxidative stressors, inflammasome activation, mitochondrial
449 impairment, lipid accumulation and cellular senescence (*4, 17, 26, 59*), all pathways that can
450 accelerate AMD progression (*13, 14*). We showed that *Irak3*$^{-/-}$ mice incurred greater oxidative
451 damage, including RPE cell mitochondrial dysfunction, senescence, and early AMD-like

pathologies such as subretinal accumulation of myeloid cells, outer retinal lesions, and cell death. The focal RPE cell death seen here in *Irak3*$^{-/-}$ mice supports findings of RPE heterogeneity in mice, like humans (*60-62*) and has been observed in other murine models of retinal degeneration, such as *Ccl2/ Cx3cr1* (CX3C motif chemokine receptor 1) double knockout (DKO), *LysMCre-Socs3*$^{fl/fl}$*Cx3cr1*$^{gfp/gfp}$ DKO, and systemic injection of sodium iodate (*63-65*).

Differential expression of IRAK-M is context-dependent in different disease settings. For instance, upregulation of IRAK-M was identified following ischemia-reperfusion of liver and brain (*66, 67*), and in infarcted heart (*68*), where it was thought to limit the magnitude of immune responses and repair pro-inflammatory damage. In a mouse model of cerebral ischemia, IRAK-M was induced by hypoxia inducible factor 1 subunit alpha (HIF1α) and played a neuroprotective role by inhibition of NF-κB signaling and production of cyclooxygenase 2 (COX2), TNF-α, NLRP3 and inducible nitric oxide synthase (iNOS). In comparison, *Irak3*$^{-/-}$ mice developed exacerbated infarcts (58). In contrast to acute responses, downregulation of IRAK-M expression was associated with chronic diseases, exemplified by alcoholic liver disease, inflammatory bowel disease, insulin resistance and metabolic syndrome (*25, 30, 31*). Indeed, although acute alcohol intake increases IRAK-M abundance in human monocytes, chronic alcohol exposure results in decreased abundance and enhanced inflammation (*69*). In obese patients, reduced *IRAK3* expression in monocytes and adipose tissues leads to mitochondrial oxidative stress and systemic inflammation (*31*). Furthermore, age-related decreases in the basal expression of IRAK-M and its inducibility upon TLR activation have been discovered in peripheral blood mononuclear cells and fibroblasts in rodents (*70, 71*). We localized the decline in IRAK-M expression to the RPE, rather than to the retina or choroid, in aging, oxidative stress and AMD , and increasing IRAK-M in the RPE via boosting endogenous gene expression or exogenous gene delivery helped to maintain mitochondrial activity and autophagy and inhibit cellular senescence and NF-κB activity, supporting the importance of IRAK-M for RPE health.

Several limitations exist in this study. Firstly, the influence of rhythmic/circadian photoreceptor outer segment phagocytosis on IRAK-M abundance in the RPE remains unknown. Given the challenges in obtaining consecutive human postmortem RPE samples for circadian analysis, collecting murine RPE samples during daytime and nighttime intervals could offer insights into this investigation for expression and gene regulation. Secondly, we cannot rule out a potential contribution of IRAK-M from other cell types to outer retinal degeneration. Conditional knockout mice via Cre/loxP or CRISPR/Cas9 will be essential for discerning pathologies arising from IRAK-M deficiency or inactivation in specific cell types, for example the RPE or retinal microglia. Thirdly, due to restricted availability of human donor eyes, we could not pinpoint the specific stage of AMD at which IRAK-M abundance is predominantly affected. Fourthly, our in vivo assessment did not show ocular toxicity when overexpressing IRAK-M for more than 6 months in *Irak3*$^{-/-}$ mice. However, it should be noted that all murine models of retinal degeneration, including the *Irak3*$^{-/-}$ mice and the murine LIRD model, do not exactly phenocopy human AMD (*72*); for pre-clinical safety and efficacy assessment, large animal studies will be required. Lastly, while early passage of ARPE-19 cell line shares RPE features, they are not fully differentiated RPE cells. Data from ARPE-19 should be used to supplement findings from human samples, in vivo and primary cell experiments.

In conclusion, we have identified an age-related decline of IRAK-M abundance, largely restricted to the RPE, which is worsened in AMD. Our findings suggest that IRAK-M plays a crucial role to maintain RPE cell homeostasis and function via co-targeting mitochondrial health, oxidative stress, autophagy and inflammation. Gene augmentation of IRAK-M demonstrates translational benefit in counteracting side-effects of aging or oxidative stress and reducing outer retinal degeneration in preclinical disease models, suggesting a therapeutic strategy via manipulating IRAK-M in the RPE in patients with AMD.

MATERIALS AND METHODS

Study design

The overall goals of this study were to define IRAK-M expression in RPE during the aging process and in AMD. The subsequent goal was to develop a targeted gene therapy for age-related and inflammation-driven RPE and retinal degeneration. For investigations on human ocular samples in all respective institutions, experiments were conducted according to the Declaration of Helsinki principles and in compliance with approved institutional guidelines. All animal protocols were approved by University of Bristol Ethical Review Group. The primary experimental procedures are described below, with detailed descriptions listed in the Supplementary Materials and Methods.

For Microarray analyses of age-related progressive changes in mRNA expression of IRAKs in human ocular samples, donor ages ranged from 35 to 97 years old (mostly between 65-85). Samples were collected from donors without clinically recorded AMD (color fundus and/or OCT imaging) where patient medical files could be queried . For donor eye tissue samples where no ocular history was available, we carefully analyzed the macular region of dissected globes under a dissecting microscope for drusen, RPE hyperpigmentation and indications of CNV bleeding. Samples were processed and run on a microarray platform in a random non-sequential order. All samples were given a random sample number and blinded to all scientists. For age-dependent results, the sample identity was unknown and only microarray gene probe name, intensity and age were compared. Inclusion required ocular tissue samples with no clinically recorded or obvious tissue AMD pathology and total mRNA RIN scores $\geqslant 7$. Samples that had obvious AMD or RIN scores <7 were excluded from these analyses.

Age- or AMD-related changes of IRAK-M protein expression in human ocular tissues were determined by Western blot or immunohistochemistry using postmortem eye tissues or paraffin-

embedded sections, respectively. The absence of other co-morbid ocular diseases or clinically-classified AMD stage of individual donor eye sample was identified by eye banks (see Supplementary Materials) according to the medical records. Sections from donor eyes diagnosed with wet AMD were excluded in the immunohistochemistry study. All samples were randomly selected from each group for analyses.

For clinical assessment of retinal pathology in different murine models associated with aging, IRAK-M deficiency or oxidative stress, eyes were examined at indicated time points using Micron IV-guided fundoscopy and OCT and assessed by investigators blinded to the origin of images. For assessment of IRAK-M replenishment by subretinal administration of AAV2-expressing human *IRAK3* in mice, animals were randomly allocated to different treatment groups. The subretinal injection procedure created a temporary subretinal bleb, where a part of the retina was elevated and separated from the RPE to accommodate the injected fluid. Mice that had no retinal blebs immediately after the injection were excluded from the study. In all cases, null AAV2 vehicle injections served as a negative control to determine baseline tissue responses. Laterality of injected eyes was randomized, and the investigators were blinded to the vector type throughout intervention and analysis. The sample size was chosen empirically based on the results of previous studies and preliminary experiments according to the 3R principles, and varied between experimental settings. In animal experiments, we collected all samples during the daytime (lights ON between 7:00am and 7:00pm) to avoid potential day-night fluctuation. For all experiments, the number of replicates, statistical tests used, and P values are reported in the figure legends.

Human sample analyses

We used gene burden test on the GWAS data (*6*) to analyze whether there was a genetic association between rare variants of *IRAK3* and AMD, compared to other Myddosome-associated genes. Microarray analysis was used to explore age-related changes in mRNA expression of *IRAKs* in

552 extramacular and macula RPE/choroid or retina. AMD-associated changes in mRNA expression
553 of *IRAKs* and known genes involved in the negative regulation of TLR/IL-1R/MyD88/IRAK1/4
554 pathways were discerned by data mining of RNA-seq data (GSE99248). AMD-associated changes
555 in IRAK-M protein expression was examined by immunohistochemistry of postmortem eye
556 sections from patients with AMD or age-matched controls. The processing and staining of all
557 sections were executed at the same time with the same vials of reagents and antibody to avoid
558 batch effects.
559
560 **_Irak3_$^{-/-}$, aging mice and oxidative stress induction**
561 We used *Irak3*$^{-/-}$ and WT mice to define whether ageing and/or lack of *I*RAK-M affected outer
562 retinal degeneration. Only male mice from the established *Rd8*-negative *Irak3*$^{-/-}$ colony were used
563 to avoid possible sex-associated variation in immune responsiveness (*73*). Clinical examinations
564 on retinal pathology, including retinal structure, fundus spots and thickness, were performed using
565 Micron IV-guided fundoscopy and optical coherence tomography (OCT) in *Irak3*$^{-/-}$ mice (aged 2-
566 15 months) and WT mice (aged 2-21 months). Primary endpoints were RPE cell death, subretinal
567 accumulation of macrophages, and cytokine expression at indicated time points. To determine
568 whether oxidative stress could be an independent factor affecting IRAK-M expression, we applied
569 oxidative stressors to different RPE cells in vitro and 8-week-old WT mice in vivo. Two types of
570 LIRD model with different severity of outer retinal injury were performed via fundus camera-
571 directed light exposure using either a light-only protocol (100 klux for 20 minutes), or a FL-
572 assisted light challenge protocol where overnight dark adapted mice were intraperitoneally
573 administered with 100 µl of 2% fluorescein before light challenge to the retina (16 klux for 5
574 minutes) (*46*). Paraquat-induced retinal degeneration was conducted by intravitreal injection of
575 paraquat diluted in PBS (2 µl; 1.5mM) (*47*). The contralateral eye was left without light challenge
576 or injected intravitreally with PBS as a control.

To elucidate metabolic mechanisms involved in *Irak3*-KO-induced retinal degeneration, we isolated primary RPE cells from 5-month-old *Irak3*$^{-/-}$ versus WT littermates and characterized cell metabolism and senescent phenotype. To demonstrate whether IRAK-M had a protecting role for RPE cells against oxidative or immune challenges in vitro, we overexpressed *IRAK3* by either endogenous CRISPR/Cas9 activation or exogenous *IRAK3* delivery via plasmid vectors. In vitro cell responses to stressors and *IRAK3* gene delivery were assessed for mitochondrial respiration and glycolytic activities, autophagy flux, cytokine secretion, and expression of senescence markers (see Supplementary Materials and Methods).

Therapeutic approaches

Subretinal administration of AAV2-expressing human *IRAK3* in two murine models of retinal degeneration, light-induced outer retinal degeneration in young WT mice and spontaneous outer retinal degeneration in aging *Irak3*$^{-/-}$ mice. In both models, null AAV2 vehicle injections served as a negative control to determine baseline responses. The control AAV2 and *IRAK3*-expressing AAV2 were both under the control of constitutive CMV or RPE-specific Best1 promoter. A pilot experiment to determine viral dose-dependent transduction efficacy was performed by subretinal injection of 2×10^9 gc (high dose) or 4×10^8 gc (low dose) of AAV2.CMV.EGFP to each eye and evaluated by fundal fluorescence imaging for 11 weeks. AAV-mediated human *IRAK3* transgene expression in mice RPE/retina was verified by qRT-PCR and immunohistochemistry of retinal samples. Retinas were exposed to light challenge at two (LIRD) or three (FL- LIRD) weeks after AAV injection, and retinal pathologies were examined two weeks after AAV injection by fundoscopy, OCT, and histology for TUNEL$^+$ cell death and mitochondrial content. *Irak3* $^{-/-}$ mice (2-4m old) were monitored for 6 months following subretinal injection of AAV vectors using quantitative parameters such as retinal fundus spots and outer retinal thickness, measured by fundoscopy and OCT.

Statistics

Results are presented as means ± standard deviation (SD). A simple linear regression was utilized using GraphPad Prism 9.5 to analyze the correlation between gene expression and human aging using microarray data. All other statistical analyses were conducted using Prism 10.1.2. All primary data associated with the statistical analyses are presented in Data file S1. For data analysis on experiments with one variable, normal distribution of samples was determined using Shapiro-Wilk test, and equality in variances across groups with normal data was measured using F-test for two groups or Brown-Forsythe test for more than two groups (Data file S2). Comparison between two groups with a single variable was performed using unpaired two-tailed Student's *t*-test for normal data with equal variances, Welch's *t*-test for normal data with unequal variances, or Mann-Whitney *U*-test if at least one group has nonnormal samples. For experiments involving more than two groups and one variable, comparisons were measured using one-way analysis of variance (ANOVA) followed by Bonferroni post-hoc multiple comparisons tests if all groups are normal and equal, Brown-Forsythe and Welch ANOVA with Dunnett's T3 tests if groups are normal but unequal, or Kruskal-Wallis ANOVA with Dunn's tests if at least one group is nonnormal. In experiments involving two independent variables, we used two-way ANOVA followed by Bonferroni post-hoc tests for all human sample, in vitro, and most animal experiments. In experiments assessing the impact of acute oxidative stress (induced by light or intravitreal injection of paraquat) on murine retinal thickness (Fig. 4, C, F and G), Holm-Sidak post-hoc tests were employed to enhance statistical power and minimize the need for additional animals in the experiments. For two-way ANOVA, certain degrees of nonnormally distributed data can be tolerated by ANOVA, which is robust to violations of normality (*74, 75*). All specific statistical tests and post-hoc methods are specified in figure legends. Differences between groups were considered significant at $P < 0.05$.

LIST OF SUPPLEMENTARY MATERIALS

Materials and Methods

Figs. S1 to S14

Table S1 and S2

Data files S1 and S2

References (*76-82*)

REFERENCES

1. J. Moretti, J. M. Blander, Cell-autonomous stress responses in innate immunity. *J Leukoc Biol* **101**, 77-86 (2017).
2. C. Franceschi, P. Garagnani, P. Parini, C. Giuliani, A. Santoro, Inflammaging: a new immune-metabolic viewpoint for age-related diseases. *Nat Rev Endocrinol* **14**, 576-590 (2018).
3. Y. Tong, S. Wang, Not All Stressors Are Equal: Mechanism of Stressors on RPE Cell Degeneration. *Front Cell Dev Biol* **8**, 591067 (2020).
4. D. A. Copland, S. Theodoropoulou, J. Liu, A. D. Dick, A Perspective of AMD Through the Eyes of Immunology. *Invest Ophthalmol Vis Sci* **59**, AMD83-AMD92 (2018).
5. J. T. Handa, C. Bowes Rickman, A. D. Dick, M. B. Gorin, J. W. Miller, C. A. Toth, M. Ueffing, M. Zarbin, L. A. Farrer, A systems biology approach towards understanding and treating non-neovascular age-related macular degeneration. *Nat Commun* **10**, 3347 (2019).
6. L. G. Fritsche, W. Igl, J. N. Bailey, F. Grassmann, S. Sengupta, J. L. Bragg-Gresham, K. P. Burdon, S. J. Hebbring, C. Wen, M. Gorski, I. K. Kim, D. Cho, D. Zack, E. Souied, H. P. Scholl, E. Bala, K. E. Lee, D. J. Hunter, R. J. Sardell, P. Mitchell, J. E. Merriam, V. Cipriani, J. D. Hoffman, T. Schick, Y. T. Lechanteur, R. H. Guymer, M. P. Johnson, Y. Jiang, C. M. Stanton, G. H. Buitendijk, X. Zhan, A. M. Kwong, A. Boleda, M. Brooks, L. Gieser, R. Ratnapriya, K. E. Branham, J. R. Foerster, J. R. Heckenlively, M. I. Othman, B. J. Vote, H. H. Liang, E. Souzeau, I. L. McAllister, T. Isaacs, J. Hall, S. Lake, D. A. Mackey, I. J. Constable, J. E. Craig, T. E. Kitchner, Z. Yang, Z. Su, H. Luo, D. Chen, H. Ouyang, K. Flagg, D. Lin, G. Mao, H. Ferreyra, K. Stark, C. N. von Strachwitz, A. Wolf, C. Brandl, G. Rudolph, M. Olden, M. A. Morrison, D. J. Morgan, M. Schu, J. Ahn, G. Silvestri, E. E. Tsironi, K. H. Park, L. A. Farrer, A. Orlin, A. Brucker, M. Li, C. A. Curcio, S. Mohand-Saïd, J. A. Sahel, I. Audo, M. Benchaboune, A. J. Cree, C. A. Rennie, S. V. Goverdhan, M. Grunin, S. Hagbi-Levi, P. Campochiaro, N. Katsanis, F. G. Holz, F. Blond, H. Blanché, J. F. Deleuze, R. P. Igo, B. Truitt, N. S. Peachey, S. M. Meuer, C. E. Myers, E. L. Moore, R. Klein, M. A. Hauser, E. A. Postel, M. D. Courtenay, S. G.

Schwartz, J. L. Kovach, W. K. Scott, G. Liew, A. G. Tan, B. Gopinath, J. C. Merriam, R. T. Smith, J. C. Khan, H. Shahid, A. T. Moore, J. A. McGrath, R. Laux, M. A. Brantley, A. Agarwal, L. Ersoy, A. Caramoy, T. Langmann, N. T. Saksens, E. K. de Jong, C. B. Hoyng, M. S. Cain, A. J. Richardson, T. M. Martin, J. Blangero, D. E. Weeks, B. Dhillon, C. M. van Duijn, K. F. Doheny, J. Romm, C. C. Klaver, C. Hayward, M. B. Gorin, M. L. Klein, P. N. Baird, A. I. den Hollander, S. Fauser, J. R. Yates, R. Allikmets, J. J. Wang, D. A. Schaumberg, B. E. Klein, S. A. Hagstrom, I. Chowers, A. J. Lotery, T. Léveillard, K. Zhang, M. H. Brilliant, A. W. Hewitt, A. Swaroop, E. Y. Chew, M. A. Pericak-Vance, M. DeAngelis, D. Stambolian, J. L. Haines, S. K. Iyengar, B. H. Weber, G. R. Abecasis, I. M. Heid, A large genome-wide association study of age-related macular degeneration highlights contributions of rare and common variants. *Nat Genet* **48**, 134-143 (2016).

7. T. W. Winkler, F. Grassmann, C. Brandl, C. Kiel, F. Günther, T. Strunz, L. Weidner, M. E. Zimmermann, C. A. Korb, A. Poplawski, A. K. Schuster, M. Müller-Nurasyid, A. Peters, F. G. Rauscher, T. Elze, K. Horn, M. Scholz, M. Cañadas-Garre, A. J. McKnight, N. Quinn, R. E. Hogg, H. Küchenhoff, I. M. Heid, K. J. Stark, B. H. F. Weber, Genome-wide association meta-analysis for early age-related macular degeneration highlights novel loci and insights for advanced disease. *BMC Med Genomics* **13**, 120 (2020).
8. H. Khan, A. A. Aziz, H. Sulahria, A. Ahmed, N. Choudhry, R. Narayanan, C. Danzig, A. M. Khanani, Emerging Treatment Options for Geographic Atrophy (GA) Secondary to Age-Related Macular Degeneration. *Clin Ophthalmol* **17**, 321-327 (2023).
9. B. L. Yaspan, D. F. Williams, F. G. Holz, C. D. Regillo, Z. Li, A. Dressen, M. van Lookeren Campagne, K. N. Le, R. R. Graham, T. Beres, T. R. Bhangale, L. A. Honigberg, A. Smith, E. C. Henry, C. Ho, E. C. Strauss, M. S. Investigators, Targeting factor D of the alternative complement pathway reduces geographic atrophy progression secondary to age-related macular degeneration. *Sci Transl Med* **9**, (2017).
10. B. Calippe, S. Augustin, F. Beguier, H. Charles-Messance, L. Poupel, J. B. Conart, S. J. Hu, S. Lavalette, A. Fauvet, J. Rayes, O. Levy, W. Raoul, C. Fitting, T. Denèfle, M. C. Pickering, C. Harris, S. Jorieux, P. M. Sullivan, J. A. Sahel, P. Karoyan, P. Sapieha, X. Guillonneau, E. L. Gautier, F. Sennlaub, Complement Factor H Inhibits CD47-Mediated Resolution of Inflammation. *Immunity* **46**, 261-272 (2017).
11. F. Beguier, M. Housset, C. Roubeix, S. Augustin, Y. Zagar, C. Nous, T. Mathis, C. Eandi, M. Benchaboune, A. Drame-Maigné, W. Carpentier, S. Chardonnet, S. Touhami, G. Blot, J. B. Conart, H. Charles-Messance, A. Potey, J. F. Girmens, M. Paques, F. Blond, T. Leveillard, E. Koertvely, J. E. Roger, J. A. Sahel, P. Sapieha, C. Delarasse, X. Guillonneau, F. Sennlaub, The 10q26 Risk Haplotype of Age-Related Macular Degeneration Aggravates Subretinal Inflammation by Impairing Monocyte Elimination. *Immunity* **53**, 429-441.e428 (2020).
12. C. B. Toomey, U. Kelly, D. R. Saban, C. Bowes Rickman, Regulation of age-related macular degeneration-like pathology by complement factor H. *Proc Natl Acad Sci U S A* **112**, E3040-3049 (2015).
13. S. Romero-Vazquez, V. Llorens, A. Soler-Boronat, M. Figueras-Roca, A. Adan, B. Molins, Interlink between Inflammation and Oxidative Stress in Age-Related Macular Degeneration: Role of Complement Factor H. *Biomedicines* **9**, (2021).
14. W. A. Tseng, T. Thein, K. Kinnunen, K. Lashkari, M. S. Gregory, P. A. D'Amore, B. R. Ksander, NLRP3 inflammasome activation in retinal pigment epithelial cells by lysosomal destabilization: implications for age-related macular degeneration. *Invest Ophthalmol Vis Sci* **54**, 110-120 (2013).
15. A. Klettner, J. Roider, Retinal Pigment Epithelium Expressed Toll-like Receptors and Their Potential Role in Age-Related Macular Degeneration. *Int J Mol Sci* **22**, (2021).

16. V. Tarallo, Y. Hirano, B. D. Gelfand, S. Dridi, N. Kerur, Y. Kim, W. G. Cho, H. Kaneko, B. J. Fowler, S. Bogdanovich, R. J. Albuquerque, W. W. Hauswirth, V. A. Chiodo, J. F. Kugel, J. A. Goodrich, S. L. Ponicsan, G. Chaudhuri, M. P. Murphy, J. L. Dunaief, B. K. Ambati, Y. Ogura, J. W. Yoo, D. K. Lee, P. Provost, D. R. Hinton, G. Núñez, J. Z. Baffi, M. E. Kleinman, J. Ambati, DICER1 loss and Alu RNA induce age-related macular degeneration via the NLRP3 inflammasome and MyD88. *Cell* **149**, 847-859 (2012).
17. K. S. Lee, S. Lin, D. A. Copland, A. D. Dick, J. Liu, Cellular senescence in the aging retina and developments of senotherapies for age-related macular degeneration. *J Neuroinflammation* **18**, 32 (2021).
18. K. Mulfaul, M. Rhatigan, S. Doyle, Toll-Like Receptors and Age-Related Macular Degeneration. *Adv Exp Med Biol* **1074**, 19-28 (2018).
19. L. Ma, F. Y. Tang, W. K. Chu, A. L. Young, M. E. Brelen, C. P. Pang, L. J. Chen, Association of toll-like receptor 3 polymorphism rs3775291 with age-related macular degeneration: a systematic review and meta-analysis. *Sci Rep* **6**, 19718 (2016).
20. M. Hata, E. M. M. A. Andriessen, R. Diaz-Marin, F. Fournier, S. Crespo-Garcia, G. Blot, R. Juneau, F. Pilon, A. Dejda, V. Guber, E. Heckel, C. Daneault, V. Calderon, C. Des Rosiers, H. J. Melichar, T. Langmann, J. S. Joyal, A. M. Wilson, P. Sapieha, Past history of obesity triggers persistent epigenetic changes in innate immunity and exacerbates neuroinflammation. *Science* **379**, 45-62 (2023).
21. M. Kader, M. Alaoui-El-Azher, J. Vorhauer, B. B. Kode, J. Z. Wells, D. Stolz, G. Michalopoulos, A. Wells, M. Scott, N. Ismail, MyD88-dependent inflammasome activation and autophagy inhibition contributes to Ehrlichia-induced liver injury and toxic shock. *PLoS Pathog* **13**, e1006644 (2017).
22. S. Wang, Y. Zheng, Q. Li, X. He, R. Ren, W. Zhang, M. Song, H. Hu, F. Liu, G. Sun, S. Sun, Z. Liu, Y. Yu, P. Chan, G. G. Zhao, Q. Zhou, G. H. Liu, F. Tang, J. Qu, Deciphering primate retinal aging at single-cell resolution. *Protein Cell* **12**, 889-898 (2021).
23. J. Liu, D. A. Copland, S. Theodoropoulou, H. A. Chiu, M. D. Barba, K. W. Mak, M. Mack, L. B. Nicholson, A. D. Dick, Impairing autophagy in retinal pigment epithelium leads to inflammasome activation and enhanced macrophage-mediated angiogenesis. *Sci Rep* **6**, 20639 (2016).
24. A. J. Clare, J. Liu, D. A. Copland, S. Theodoropoulou, A. D. Dick, Unravelling the therapeutic potential of IL-33 for atrophic AMD. *Eye (Lond)*, (2021).
25. A. Jain, S. Kaczanowska, E. Davila, IL-1 Receptor-Associated Kinase Signaling and Its Role in Inflammation, Cancer Progression, and Therapy Resistance. *Front Immunol* **5**, 553 (2014).
26. R. Gill, A. Tsung, T. Billiar, Linking oxidative stress to inflammation: Toll-like receptors. *Free Radic Biol Med* **48**, 1121-1132 (2010).
27. J. Du, G. A. Nicolaes, D. Kruijswijk, M. Versloot, T. van der Poll, C. van 't Veer, The structure function of the death domain of human IRAK-M. *Cell Commun Signal* **12**, 77 (2014).
28. H. Zhou, M. Yu, K. Fukuda, J. Im, P. Yao, W. Cui, K. Bulek, J. Zepp, Y. Wan, T. W. Kim, W. Yin, V. Ma, J. Thomas, J. Gu, J. A. Wang, P. E. DiCorleto, P. L. Fox, J. Qin, X. Li, IRAK-M mediates Toll-like receptor/IL-1R-induced NFκB activation and cytokine production. *EMBO J* **32**, 583-596 (2013).
29. K. Lyroni, A. Patsalos, M. G. Daskalaki, C. Doxaki, B. Soennichsen, M. Helms, I. Liapis, V. Zacharioudaki, S. C. Kampranis, C. Tsatsanis, Epigenetic and Transcriptional Regulation of IRAK-M Expression in Macrophages. *J Immunol* **198**, 1297-1307 (2017).
30. L. L. Hubbard, B. B. Moore, IRAK-M regulation and function in host defense and immune homeostasis. *Infect Dis Rep* **2**, (2010).

31. M. Hulsmans, B. Geeraert, D. De Keyzer, A. Mertens, M. Lannoo, B. Vanaudenaerde, M. Hoylaerts, N. Benhabiles, C. Tsatsanis, C. Mathieu, P. Holvoet, Interleukin-1 receptor-associated kinase-3 is a key inhibitor of inflammation in obesity and metabolic syndrome. *PLoS One* **7**, e30414 (2012).
32. L. Balaci, M. C. Spada, N. Olla, G. Sole, L. Loddo, F. Anedda, S. Naitza, M. A. Zuncheddu, A. Maschio, D. Altea, M. Uda, S. Pilia, S. Sanna, M. Masala, L. Crisponi, M. Fattori, M. Devoto, S. Doratiotto, S. Rassu, S. Mereu, E. Giua, N. G. Cadeddu, R. Atzeni, U. Pelosi, A. Corrias, R. Perra, P. L. Torrazza, P. Pirina, F. Ginesu, S. Marcias, M. G. Schintu, G. S. Del Giacco, P. E. Manconi, G. Malerba, A. Bisognin, E. Trabetti, A. Boner, L. Pescollderungg, P. F. Pignatti, D. Schlessinger, A. Cao, G. Pilia, IRAK-M is involved in the pathogenesis of early-onset persistent asthma. *Am J Hum Genet* **80**, 1103-1114 (2007).
33. L. M. Scott, E. E. Vincent, N. Hudson, C. Neal, N. Jones, E. C. Lavelle, M. Campbell, A. P. Halestrap, A. D. Dick, S. Theodoropoulou, Interleukin-33 regulates metabolic reprogramming of the retinal pigment epithelium in response to immune stressors. *JCI Insight* **6**, (2021).
34. H. Xi, K. J. Katschke, Y. Li, T. Truong, W. P. Lee, L. Diehl, L. Rangell, J. Tao, R. Arceo, J. Eastham-Anderson, J. A. Hackney, A. Iglesias, J. Cote-Sierra, J. Elstrott, R. M. Weimer, M. van Lookeren Campagne, IL-33 amplifies an innate immune response in the degenerating retina. *J Exp Med* **213**, 189-207 (2016).
35. J. Augustine, S. Pavlou, I. Ali, K. Harkin, E. Ozaki, M. Campbell, A. W. Stitt, H. Xu, M. Chen, IL-33 deficiency causes persistent inflammation and severe neurodegeneration in retinal detachment. *J Neuroinflammation* **16**, 251 (2019).
36. E. J. Kim, G. R. Grant, A. S. Bowman, N. Haider, H. V. Gudiseva, V. R. M. Chavali, Complete Transcriptome Profiling of Normal and Age-Related Macular Degeneration Eye Tissues Reveals Dysregulation of Anti-Sense Transcription. *Sci Rep* **8**, 3040 (2018).
37. J. Tode, E. Richert, S. Koinzer, A. Klettner, C. von der Burchard, R. Brinkmann, R. Lucius, J. Roider, Selective Retina Therapy Reduces Bruch's Membrane Thickness and Retinal Pigment Epithelium Pathology in Age-Related Macular Degeneration Mouse Models. *Transl Vis Sci Technol* **8**, 11 (2019).
38. D. E. Rothschild, Y. Zhang, N. Diao, C. K. Lee, K. Chen, C. C. Caswell, D. J. Slade, R. F. Helm, T. LeRoith, L. Li, I. C. Allen, Enhanced Mucosal Defense and Reduced Tumor Burden in Mice with the Compromised Negative Regulator IRAK-M. *EBioMedicine* **15**, 36-47 (2017).
39. K. Kobayashi, L. D. Hernandez, J. E. Galán, C. A. Janeway, R. Medzhitov, R. A. Flavell, IRAK-M is a negative regulator of Toll-like receptor signaling. *Cell* **110**, 191-202 (2002).
40. S. M. Lange, M. I. Nelen, P. Cohen, Y. Kulathu, Dimeric Structure of the Pseudokinase IRAK3 Suggests an Allosteric Mechanism for Negative Regulation. *Structure* **29**, 238-251.e234 (2021).
41. P. Herrmann, J. A. Cowing, E. Cristante, S. E. Liyanage, J. Ribeiro, Y. Duran, L. Abelleira Hervas, L. S. Carvalho, J. W. Bainbridge, U. F. Luhmann, R. R. Ali, Cd59a deficiency in mice leads to preferential innate immune activation in the retinal pigment epithelium-choroid with age. *Neurobiol Aging* **36**, 2637-2648 (2015).
42. N. K. Wang, H. F. Fine, S. Chang, C. L. Chou, W. Cella, J. Tosi, C. S. Lin, T. Nagasaki, S. H. Tsang, Cellular origin of fundus autofluorescence in patients and mice with a defective NR2E3 gene. *Br J Ophthalmol* **93**, 1234-1240 (2009).
43. N. L. Hawes, B. Chang, G. S. Hageman, S. Nusinowitz, P. M. Nishina, B. S. Schneider, R. S. Smith, T. H. Roderick, M. T. Davisson, J. R. Heckenlively, Retinal degeneration 6

(rd6): a new mouse model for human retinitis punctata albescens. *Invest Ophthalmol Vis Sci* **41**, 3149-3157 (2000).
44. G. Venturini, D. Kokona, B. L. Steiner, E. G. Bulla, J. Jovanovic, M. S. Zinkernagel, P. Escher, In vivo analysis of onset and progression of retinal degeneration in the Nr2e3. *Sci Rep* **11**, 19032 (2021).
45. K. Makabe, S. Sugita, M. Mandai, Y. Futatsugi, M. Takahashi, Microglia dynamics in retinitis pigmentosa model: formation of fundus whitening and autofluorescence as an indicator of activity of retinal degeneration. *Sci Rep* **10**, 14700 (2020).
46. Y. Ding, B. Aredo, X. Zhong, C. X. Zhao, R. L. Ufret-Vincenty, Increased susceptibility to fundus camera-delivered light-induced retinal degeneration in mice deficient in oxidative stress response proteins. *Exp Eye Res* **159**, 58-68 (2017).
47. C. Cingolani, B. Rogers, L. Lu, S. Kachi, J. Shen, P. A. Campochiaro, Retinal degeneration from oxidative damage. *Free Radic Biol Med* **40**, 660-669 (2006).
48. P. Jin, L. Bo, Y. Liu, W. Lu, S. Lin, J. Bian, X. Deng, Activator protein 1 promotes the transcriptional activation of IRAK-M. *Biomed Pharmacother* **83**, 1212-1219 (2016).
49. M. A. Kanow, M. M. Giarmarco, C. S. Jankowski, K. Tsantilas, A. L. Engel, J. Du, J. D. Linton, C. C. Farnsworth, S. R. Sloat, A. Rountree, I. R. Sweet, K. J. Lindsay, E. D. Parker, S. E. Brockerhoff, M. Sadilek, J. R. Chao, J. B. Hurley, Biochemical adaptations of the retina and retinal pigment epithelium support a metabolic ecosystem in the vertebrate eye. *Elife* **6**, (2017).
50. S. Russell, J. Bennett, J. A. Wellman, D. C. Chung, Z. F. Yu, A. Tillman, J. Wittes, J. Pappas, O. Elci, S. McCague, D. Cross, K. A. Marshall, J. Walshire, T. L. Kehoe, H. Reichert, M. Davis, L. Raffini, L. A. George, F. P. Hudson, L. Dingfield, X. Zhu, J. A. Haller, E. H. Sohn, V. B. Mahajan, W. Pfeifer, M. Weckmann, C. Johnson, D. Gewaily, A. Drack, E. Stone, K. Wachtel, F. Simonelli, B. P. Leroy, J. F. Wright, K. A. High, A. M. Maguire, Efficacy and safety of voretigene neparvovec (AAV2-hRPE65v2) in patients with RPE65-mediated inherited retinal dystrophy: a randomised, controlled, open-label, phase 3 trial. *Lancet* **390**, 849-860 (2017).
51. L. H. Vandenberghe, P. Bell, A. M. Maguire, C. N. Cearley, R. Xiao, R. Calcedo, L. Wang, M. J. Castle, A. C. Maguire, R. Grant, J. H. Wolfe, J. M. Wilson, J. Bennett, Dosage thresholds for AAV2 and AAV8 photoreceptor gene therapy in monkey. *Sci Transl Med* **3**, 88ra54 (2011).
52. S. Koponen, E. Kokki, T. Tamminen, S. Ylä-Herttuala, AAV2 and AAV9 tropism and transgene expression in the mouse eye and major tissues after intravitreal and subretinal delivery. *Frontiers in Drug Delivery* **3**, (2023).
53. Y. B. Johari, A. C. Mercer, Y. Liu, A. J. Brown, D. C. James, Design of synthetic promoters for controlled expression of therapeutic genes in retinal pigment epithelial cells. *Biotechnol Bioeng* **118**, 2001-2015 (2021).
54. D. M. Wu, X. Ji, M. V. Ivanchenko, M. Chung, M. Piper, P. Rana, S. K. Wang, Y. Xue, E. West, S. R. Zhao, H. Xu, M. Cicconet, W. Xiong, C. L. Cepko, Nrf2 overexpression rescues the RPE in mouse models of retinitis pigmentosa. *JCI Insight* **6**, (2021).
55. J. J. Hunter, J. I. Morgan, W. H. Merigan, D. H. Sliney, J. R. Sparrow, D. R. Williams, The susceptibility of the retina to photochemical damage from visible light. *Prog Retin Eye Res* **31**, 28-42 (2012).
56. K. Yokoo, Y. Yamamoto, T. Suzuki, Ammonia impairs tight junction barriers by inducing mitochondrial dysfunction in Caco-2 cells. *FASEB J* **35**, e21854 (2021).
57. M. Zhang, W. Chen, W. Zhou, Y. Bai, J. Gao, Critical Role of IRAK-M in Regulating Antigen-Induced Airway Inflammation. *Am J Respir Cell Mol Biol* **57**, 547-559 (2017).
58. Y. Ma, R. L. Haynes, R. L. Sidman, T. Vartanian, TLR8: an innate immune receptor in brain, neurons and axons. *Cell Cycle* **6**, 2859-2868 (2007).

59. K. Kaarniranta, H. Uusitalo, J. Blasiak, S. Felszeghy, R. Kannan, A. Kauppinen, A. Salminen, D. Sinha, D. Ferrington, Mechanisms of mitochondrial dysfunction and their impact on age-related macular degeneration. *Prog Retin Eye Res* **79**, 100858 (2020).
60. D. Ortolan, R. Sharma, A. Volkov, A. Maminishkis, N. A. Hotaling, L. A. Huryn, C. Cukras, S. Di Marco, S. Bisti, K. Bharti, Single-cell-resolution map of human retinal pigment epithelium helps discover subpopulations with differential disease sensitivity. *Proc Natl Acad Sci U S A* **119**, e2117553119 (2022).
61. H. Lee, H. Y. Lee, J. B. Chae, C. W. Park, C. Kim, J. H. Ryu, J. Jang, N. Kim, H. Chung, Single-cell transcriptome of the mouse retinal pigment epithelium in response to a low-dose of doxorubicin. *Commun Biol* **5**, 722 (2022).
62. S. Datta, M. Cano, G. Satyanarayana, T. Liu, L. Wang, J. Wang, J. Cheng, K. Itoh, A. Sharma, I. Bhutto, R. Kannan, J. Qian, D. Sinha, J. T. Handa, Mitophagy initiates retrograde mitochondrial-nuclear signaling to guide retinal pigment cell heterogeneity. *Autophagy* **19**, 966-983 (2023).
63. X. Du, E. M. Byrne, M. Chen, H. Xu, Minocycline Inhibits Microglial Activation and Improves Visual Function in a Chronic Model of Age-Related Retinal Degeneration. *Biomedicines* **10**, (2022).
64. J. Tuo, C. M. Bojanowski, M. Zhou, D. Shen, R. J. Ross, K. I. Rosenberg, D. J. Cameron, C. Yin, J. A. Kowalak, Z. Zhuang, K. Zhang, C. C. Chan, Murine ccl2/cx3cr1 deficiency results in retinal lesions mimicking human age-related macular degeneration. *Invest Ophthalmol Vis Sci* **48**, 3827-3836 (2007).
65. A. Enzbrenner, R. Zulliger, J. Biber, A. M. Q. Pousa, N. Schäfer, C. Stucki, N. Giroud, M. Berrera, E. Kortvely, R. Schmucki, L. Badi, A. Grosche, D. Pauly, V. Enzmann, Sodium Iodate-Induced Degeneration Results in Local Complement Changes and Inflammatory Processes in Murine Retina. *Int J Mol Sci* **22**, (2021).
66. W. Li, R. Huang, X. Gong, Z. Zhao, L. Zhang, Q. Zhou, X. Jiang, H. Tie, J. Wan, B. Wang, Allicin attenuated hepatic ischemia/reperfusion injury in mice by regulating PPARγ-IRAK-M-TLR4 signal pathway. *Food Funct* **13**, 7361-7376 (2022).
67. C. Lyu, Y. Zhang, M. Gu, Y. Huang, G. Liu, C. Wang, M. Li, S. Chen, S. Pan, Y. Gu, IRAK-M Deficiency Exacerbates Ischemic Neurovascular Injuries in Experimental Stroke Mice. *Front Cell Neurosci* **12**, 504 (2018).
68. A. Saxena, A. V. Shinde, Z. Haque, Y. J. Wu, W. Chen, Y. Su, N. G. Frangogiannis, The role of Interleukin Receptor Associated Kinase (IRAK)-M in regulation of myofibroblast phenotype in vitro, and in an experimental model of non-reperfused myocardial infarction. *J Mol Cell Cardiol* **89**, 223-231 (2015).
69. P. Mandrekar, S. Bala, D. Catalano, K. Kodys, G. Szabo, The opposite effects of acute and chronic alcohol on lipopolysaccharide-induced inflammation are linked to IRAK-M in human monocytes. *J Immunol* **183**, 1320-1327 (2009).
70. Y. Li, E. A. Howell, A. S. Lagoo, M. Kuchibhatla, H. Pan, H. J. Cohen, S. A. Lagoo, Differential gene expression of interleukin-1 receptor associated kinase-1 and interleukin-1 receptor associated kinase-M in peripheral blood mononuclear cells of young and aged rats following preconditioning with endotoxin. *Shock* **31**, 55-63 (2009).
71. H. Domon, K. Tabeta, T. Nakajima, K. Yamazaki, Age-related alterations in gene expression of gingival fibroblasts stimulated with Porphyromonas gingivalis. *J Periodontal Res* **49**, 536-543 (2014).
72. M. E. Pennesi, M. Neuringer, R. J. Courtney, Animal models of age related macular degeneration. *Mol Aspects Med* **33**, 487-509 (2012).
73. S. L. Klein, K. L. Flanagan, Sex differences in immune responses. *Nat Rev Immunol* **16**, 626-638 (2016).

74. M. E. Harrigan, A. R. Filous, C. P. Vadala, A. Webb, M. Pietrzak, Z. Sahenk, H. Prüss, P. J. Reiser, P. G. Popovich, W. D. Arnold, J. M. Schwab, Lesion level-dependent systemic muscle wasting after spinal cord injury is mediated by glucocorticoid signaling in mice. *Sci Transl Med* **15**, eadh2156 (2023).
75. M. J. Blanca, R. Alarcón, J. Arnau, R. Bono, R. Bendayan, Non-normal data: Is ANOVA still a valid option? *Psicothema* **29**, 552-557 (2017).
76. A. L. Price, G. V. Kryukov, P. I. de Bakker, S. M. Purcell, J. Staples, L. J. Wei, S. R. Sunyaev, Pooled association tests for rare variants in exon-resequencing studies. *Am J Hum Genet* **86**, 832-838 (2010).
77. B. Chang, R. Hurd, J. Wang, P. Nishina, Survey of common eye diseases in laboratory mouse strains. *Invest Ophthalmol Vis Sci* **54**, 4974-4981 (2013).
78. R. Fernandez-Godino, D. L. Garland, E. A. Pierce, Isolation, culture and characterization of primary mouse RPE cells. *Nat Protoc* **11**, 1206-1218 (2016).
79. M. C. Marazita, A. Dugour, M. D. Marquioni-Ramella, J. M. Figueroa, A. M. Suburo, Oxidative stress-induced premature senescence dysregulates VEGF and CFH expression in retinal pigment epithelial cells: Implications for Age-related Macular Degeneration. *Redox Biol* **7**, 78-87 (2016).
80. B. J. Raveney, D. A. Copland, A. D. Dick, L. B. Nicholson, TNFR1-dependent regulation of myeloid cell function in experimental autoimmune uveoretinitis. *J Immunol* **183**, 2321-2329 (2009).
81. J. Liu, D. A. Copland, S. Horie, W. K. Wu, M. Chen, Y. Xu, B. Paul Morgan, M. Mack, H. Xu, L. B. Nicholson, A. D. Dick, Myeloid cells expressing VEGF and arginase-1 following uptake of damaged retinal pigment epithelium suggests potential mechanism that drives the onset of choroidal angiogenesis in mice. *PLoS One* **8**, e72935 (2013).
82. H. Lee, R. Purohit, A. Patel, E. Papageorgiou, V. Sheth, G. Maconachie, A. Pilat, R. J. McLean, F. A. Proudlock, I. Gottlob, In Vivo Foveal Development Using Optical Coherence Tomography. *Invest Ophthalmol Vis Sci* **56**, 4537-4545 (2015).

ACKNOWLEDGMENTS

We thank Maritza C. McIntyre, James T. Handa and Brian C. Mansfield for their helpful discussion and critical comments on the manuscript.

Funding

This work was funded by grants from Rosetrees Trust and Stoneygate Trust (Joint grant M418-F1 to ADD, JL and DAC), Underwood Trust (to ADD), Macular Society (to ADD, JL and DAC) and Sight Research UK (grant SAC052; to JL, ADD and DAC). The work was also supported by an unrestricted grant to the Moran Eye Center from Research to Prevent Blindness, Inc. and unrestricted funds from the Sharon Eccles Steele Center for Translation Medicine (to GSH). We

thank the IAMDGC, supported by the National Eye Institute of the National Institutes of Health (grant 5R01EY022310). The work of IMH was supported by the National Institutes of Health (grants RES516564 and RES511967).

Author contributions

Conceptualization: ADD, JL, YKC and LBN. Methodology: JL, ADD, YKC, GSH, IMH, MG, BR, UG, MJR, ELF, RG, PJC, DAC and LBN. Investigation: JL, YKC, DAC, AJC, MG, BTR, GSH, LS, ST, UG, KC, GS, OHB, KO, JLBP, JW, LMR and YL. Visualization: ADD, JL, YKC and LBN. Supervision: ADD, JL and YKC. Writing—original draft: JL, ADD and YKC. Writing—review & editing: all authors.

Competing interests

ADD, JL and YKC are named inventors on an International Patent Application No: PCT/EP2022/082518. ADD and YKC are co-founders of Cirrus Therapeutics and hold equity. JL and DAC hold equity in Cirrus Therapeutics. ADD is consultant for Hubble Tx, Affibody, 4 DMT, Novartis, Roche, UCB, Amilera, Janssen, ActivBio and Apellis. YKC is Consultant or Advisor to Ally Therapeutics, AlphaSights, Anjarium Biosciences, Arthur D. Little, Celestial Therapeutics, Cirrus Therapeutics, FirstThought, Pacira Biosciences, Santé, University of Bristol and Xora Innovation, and has received consulting fees and/or equity. RG is consultant for Roche, Genentech, Apellis, Novartis, and Bayer.

Data and materials availability

All data associated with this study are present in the paper or the Supplementary Materials. Genetic data analyzed for gene burden tests (Table 1 and Table S1) are accessible from the original paper (*6*) and permitted for sharing by respective Institutional Review Boards, and summary statistics

reported in the paper are archived in the database of Genotypes and Phenotypes (dbGaP) under accession phs001039.v1.p1. Microarray data used to analyze the *IRAK3*, *IRAK1* and *IRAK4* expression correlated with aging (Fig. 1C and Fig. S2) are available from G.S.H. under a material transfer agreement with the University of Utah Technology Licensing Office, Utah, United States.

Table 1. Rare protein-altering variants of *IRAK3* are associated with increasing risk of late AMD.

Gene Symbol	CHROM	Start	End	N Markers	Increasing/decreasing risk for AMD	P value
IRAK3	12	66,582,994	66,648,402	18	Increasing risk	0.012
IRAK1	X	153,278,500	153,284,192	2	Increasing risk	0.35
IRAK2	3	10,219,555	10,280,654	12	Increasing risk	0.91
IRAK4	12	44,172,041	44,177,510	3	Decreasing risk	0.22

The cumulative effect of rare protein-altering variants in the 16,144 late AMD cases versus 17,832 controls of four *IRAK* genes in the IAMDGC data was examined using gene burden test.

Figure legends

Fig. 1. IRAK-M is abundant in the RPE and its expression is reduced with age. (**A** and **B**) Confocal images of human retinal sections from a 20-year-old donor (without recorded ocular disease). Anti-RPE65 was used to stain the RPE (red, **A**), anti-rhodopsin was used to stain the photoreceptor outer segment (red, **B**), and DAPI was used to stain nuclei (white, **A** and **B**). GCL: ganglion cell layer; INL: inner nuclear layer; ONL: outer nuclear layer; POS: photoreceptor outer segment; RPE: retinal pigment epithelium; CHO: choroid. (**C**) Graphs showing relative probe intensities for *IRAK3*, *IRAK1*, and *IRAK4* in the RPE/choroid (top) and retina (bottom), according to age of donor, as assessed by microarray. (**D**) Western blots (left) and densitometry quantification (right) of IRAK-M abundance in human RPE/choroidal lysates. Donor age, sex, and eye are indicated at the top of the blot. IRAK-M abundance was normalized to β-actin (20-22y: n=4; 52-59y: n=4; 76-84y: n=6). *P < 0.05; **P < 0.01; ns, nonsignificant. Comparison by simple linear regression (C), or one-way Brown-Forsythe and Welch ANOVA test with Dunnett's T3 tests (D).

Fig. 2. IRAK-M expression in RPE is reduced in AMD. (**A**) PORT-normalized gene counts from RNA-seq data (GSE99248) of *IRAK3*, *IRAK1*, *IRAK2* and *IRAK4* in the RPE/choroid/sclera (left; n=8 AMD, pink; n=7 age-matched controls, teal) and retina (right; n=8 AMD, pink; n=8 controls, teal). (**B**) Representative IHC images (top row) of human retinal sections from two donors without AMD (non-AMD, 59-year and 97-year old, respectively), a donor with mild AMD (76-year old), and a donor with AMD at unidentified stage (85-year old) were color-deconvoluted using ImageJ to separate IRAK-M staining (red, bottom row), pigment (brown, third row) and nuclei (blue, second row). Scale bar: 100 μm. Lower magnification images are shown in fig. S5. (**C**) Quantification of mean staining intensity of the RPE, choroid, and retina for IRAK-M abundance (n=2 non-AMD young, teal; n=5 non-AMD aged, pink; n=11 AMD, orange). *P <

0.05; ns, nonsignificant. Comparison by multiple unpaired two-tailed Welch's t-tests (RPE/Cho/Scl in A) or Mann-Whitney *U*-tests (Retina in A) followed by Sidak-Bonferroni correction, or two-way ANOVA with Bonferroni post-hoc tests (C).

Fig. 3. *Irak3*$^{-/-}$ mice spontaneously display early retinal abnormalities. (**A**) Representative fundal images of *Irak3*$^{-/-}$ mouse retinas at 5m, 8m, 10m, and 13m. White spots are indicated by red arrows. (**B**) Graph showing incidence of flecked retina (number of spots > 3) in *Irak3*$^{-/-}$ mice (pink) compared to WT controls (teal) at different ages. Each value is a ratio of number of flecked retinas to total number of retinas at each time point. (**C**) Representative fundal (top) and OCT (bottom) images from 5m-old *Irak3*$^{-/-}$ mice. White spots are indicated by red arrows. Yellow double-arrow lines indicate the boundaries of outer retinal layers (ORL), blue double-arrow lines indicate the boundaries of inner retinal layers (IRL). (**D**) TUNEL staining (left) and quantification (right) of RPE/choroidal flatmounts from *Irak3*$^{-/-}$ mice (pink, n=10) versus WT controls (teal, n=8) at 5m of age. (**E**) Quantification of OCT images to assess ORL (left) and IRL (right) thickness in *Irak3*$^{-/-}$ mice (pink, n=11) and WT controls (teal, n=12) aged 12-13m. (**F**) Quantitative RT-PCR analysis of mRNA expression of *Ccl2*, *Il1b*, and *Il12* (normalized to *RPS29*) in RPE/choroid tissues from 12m-old *Irak3*$^{-/-}$ mice (pink, n=6) and WT controls (teal, n=6). *P < 0.05; **P < 0.01; ****P < 0.0001; ns, nonsignificant. Comparison by unpaired two-tailed Welch's *t*-test (D), two-way ANOVA followed by Bonferroni tests (E and F).

Fig. 4. Oxidative stress reduces IRAK-M abundance in the RPE of WT mice, and *Irak3*$^{-/-}$ mice are more vulnerable to light-induced retinal degeneration. Retinal oxidative stress was induced in 8-week-old C57BL/6J mice by either fundus-light induction (100kLux for 20min, **A**, **C** and **E**) or intravitreal administration of paraquat (2µl at 1.5mM, **B**, **D** and **F**). (**A**) Western blots (left) and densitometry (right) showing IRAK-M abundance in RPE lysate on day 7 after light

exposure (pink) compared with control (teal) (n=4). (**B**) Western blots (left) and densitometry (right) showing IRAK-M abundance in RPE lysate on day 7 after paraquat injection (pink) compared with PBS control (teal) (n=5). (**C**) Representative fundoscopy (top) and OCT images (bottom) obtained on day 14 after light exposure. (**D**) Fundoscopy (top) and OCT images (bottom) obtained on day 14 after paraquat injection. Retinal lesions are indicated by red arrows, yellow double-arrow lines indicate the thickness of outer retinal layers (ORL), and blue double-arrow lines indicate thickness of inner retinal layers (IRL). (**E)** Quantification of OCT images to assess ORL (left) and IRL (right) thickness in LIRD mice (pink, n=8) and controls (teal, n=8). (**F)** ORL (left) and IRL (right) thickness in paraquat-injected mice (pink, n=11) and PBS-injected control (teal, n=9). (**G**) Eight-week-old WT and *Irak3*$^{-/-}$ mice were subjected to retina light-induced oxidative insults. Quantification of ORL (left) and IRL (right) thickness *Irak3*$^{-/-}$ mice (pink, n=8) compared to WT controls (teal, n=16) 14 days after light induction, as assessed by averaging of temporal and nasal measurements by OCT. *P < 0.05; **P < 0.01; ***P < 0.001; ns, nonsignificant. Comparison by unpaired two-tailed Student's *t*-test (A and B), or two-way ANOVA with Holm-Sidak post-hoc tests (E, F and G).

Fig. 5. Overexpression of *IRAK3* in RPE cells supports metabolic activities and inhibits cell death against stressors. (**A** and **B**) Metabolic flux analysis of human iPSC-RPE cells transfected with *IRAK3* CRISPR activation plasmid or control plasmid for 48h, and then challenged by 30 μM H_2O_2 or 1 μg/ml LPS for 24h. OCR (**A**) and ECAR (**B**) profile (left) and parameters (right) of the iPSC-RPE cells (n=5 control plasmid group, teal; n=6 *IRAK3* activation plasmid, pink; n=4 control plasmid + H_2O_2, blue; n=7 *IRAK3* activation plasmid + H_2O_2, orange; n=3 control plasmid + LPS, lime; n=4 *IRAK3* activation plasmid + LPS, moroon). (**C**) LDH cytotoxicity analysis of mouse B6-RPE07 cells stably transfected with pUNO1-human *IRAK3* plasmid (pink) or pUNO1 control plasmid (teal) over 5 days since confluency (d1, d4, d5: n=4; d3: n=8). (**D**) Cytotoxicity assay of

stably transfected B6-RPE07 cells treated with paraquat (125 μM, n=4) or LPS (40 ng/ml, n=2) for 72h, compared to untreated cells (n=4). (**E** and **F**) Metabolic flux analysis of transfected primary mouse *Irak3*$^{-/-}$ RPE cells treated by 60 μM H_2O_2 for 24h. OCR (**E**) and ECAR (**F**) profile (left) and parameters (right) of the cells (pUNO1, teal; pUNO1-h*IRAK3*, pink; pUNO1 + H_2O_2, orange; pUNO1-h*IRAK3* + H_2O_2, brown; all n=3). *P < 0.05; **P < 0.01; ****P < 0.0001; ns, nonsignificant. Comparison by two-way ANOVA with Bonferroni post-hoc tests.

Fig. 6. Subretinal delivery of AAV2.CMV.h*IRAK3* protects against light-induced retinal damage in wild-type mice. (**A**) Two weeks after subretinal injection of AAV2.CMV.h*IRAK3* or AAV2.CMV.Null (high dose 2×10^9 gc/eye, top; low dose 4×10^8 gc/eye, bottom), RPE/choroid and retina were analyzed for human *IRAK3* expression using qRT-PCR, normalized to *RPS29* (n=5). (**B**) Retinal cryosections were examined for high dose AAV-mediated IRAK-M expression using an antibody specific to human IRAK-M (green). DAPI staining of nuclei in blue. Representative confocal images were shown. (**C to E**) Two weeks after subretinal injection with the high dose of AAV2.CMV.h*IRAK3* or AAV2.CMV.Null, each mouse was subjected to light-induced retinal degeneration in one eye, followed by assessment of retinal pathology and therapeutic response after a further two weeks. (**C**) Representative fundoscopy (top left) and OCT images (bottom left) and quantification (right) show light-induced retinal lesions (red arrows) and averaged ORL thickness in AAV2.CMV.h*IRAK3*-treated (n=10, pink) or AAV2.CMV.Null-treated (n=11, teal) mice. (**D**) Representative confocal images of TUNEL staining on retinal sections (top) and quantification (bottom) of 3 sections from each eye treated with AAV2.CMV.h*IRAK3* (pink) or AAV2.CMV.Null (teal). n=6 for light challenge groups; n=3 for control (no light challenge) groups. (**E**) Confocal images of MitoView Green staining for mitochondrial content (top, DAPI staining shown in white) and MFI measurement (bottom) in 3 different fields from two sections of each eye treated with AAV2.CMV.h*IRAK3* or

AAV2.CMV.Null. MFI analysis was performed at different retinal layers (IS: inner segment, teal; OPL: outer plexiform layer, pink; GC/IPL: ganglion cell/inner plexiform layer, orange). n=6 for light damage groups; n=3 for no light groups. **P < 0.01; ***P < 0.001; ****P < 0.0001. Comparison by two-way ANOVA followed by Bonferroni tests (C-E).

Fig. 7. Higher dose of AAV2.Best1.h*IRAK3* is required to transduce comparable expression of exogenous IRAK-M as AAV2.CMV.h*IRAK3*. (**A**) Two weeks after subretinal injection of AAV2.CMV.h*IRAK3* (2×10^9 gc/eye), AAV2.Best1.h*IRAK3* (2 or 4×10^9 gc/eye) or AAV2.CMV.Null (2 or 4×10^9 gc/eye), retinal cryosections were prepared and stained with an antibody specific to human IRAK-M. Representative confocal images show the staining of transduced human IRAK-M (green) and DAPI (blue). (**B** and **C**) Three weeks after subretinal delivery of AAV2.CMV.h*IRAK3* (2×10^9 gc/eye), AAV2.Best1.h*IRAK3* (4×10^9 gc/eye) or AAV2.CMV.Null (2 or 4×10^9 gc/eye), each mouse was subjected to a fluorescein (FL)-assisted light-induced retinal degeneration in one eye and assessment of retinal pathology and therapeutic response were undertaken two weeks later. (**B**) Representative fundoscopy (top left) and OCT images (bottom left) and quantification (right) of averaged ORL thickness (n=6-7). (**C**) Representative confocal images of RPE flatmounts stained for tight junction protein ZO-1 (green) and mitochondrial marker Tom20 (magenta). DAPI is shown in blue. Higher magnification panels on right. **P < 0.01; ****P < 0.0001; ns, nonsignificant. Comparison by two-way ANOVA followed by Bonferroni tests (B).

Fig. 8. Subretinal delivery of AAV2.CMV.h*IRAK3* prevents age-related spontaneous retinal degeneration in *Irak3*$^{-/-}$ mice. 2×10^9 gc of AAV2.CMV.h*IRAK3* were injected subretinally in one eye of each *Irak3*$^{-/-}$ mouse (2-4m old), with AAV2.CMV.Null injected subretinally into the contralateral eye. Mice were then monitored by fundoscopy and OCT for 6 months. (**A**)

Representative fundal images of 8m-old *Irak3*$^{-/-}$ mice with AAV administration at the age of 2m. Blue lines separate the retina into two sides based on the injection site (indicated by red arrows). (**B**) Time course of incidence of flecked retina in *Irak3*$^{-/-}$ mice treated with AAV2.CMV.h*IRAK3* (n=15, pink) or AAV2.CMV.Null (n=16, teal). (**C**) Numbers of retinal spots in whole retina (left) or on the injection side (right), were blind-counted for comparison between AAV2.CMV.h*IRAK3* (n=15, pink) and AAV2.CMV.Null (n=16, teal)-treated mice at 8-10m of age. (**D**) OCT quantification of ORL thickness at 0.2 mm and 0.4 mm distant from the optic nerve head in 8-10m-old *Irak3*$^{-/-}$ mice treated with AAV2.CMV.h*IRAK3* (n=15, orange), 8-10m-old *Irak3*$^{-/-}$ mice treated with AAV2.CMV.Null (n=16, pink), and WT littermates (n=12, teal) that did not receive injections. *P < 0.05; **P < 0.01; ****P < 0.0001; ns, nonsignificant. Comparison by unpaired two-tailed Mann-Whitney *U*-tests (C) or two-way ANOVA with Bonferroni post-hoc tests (D).

Fig. 1

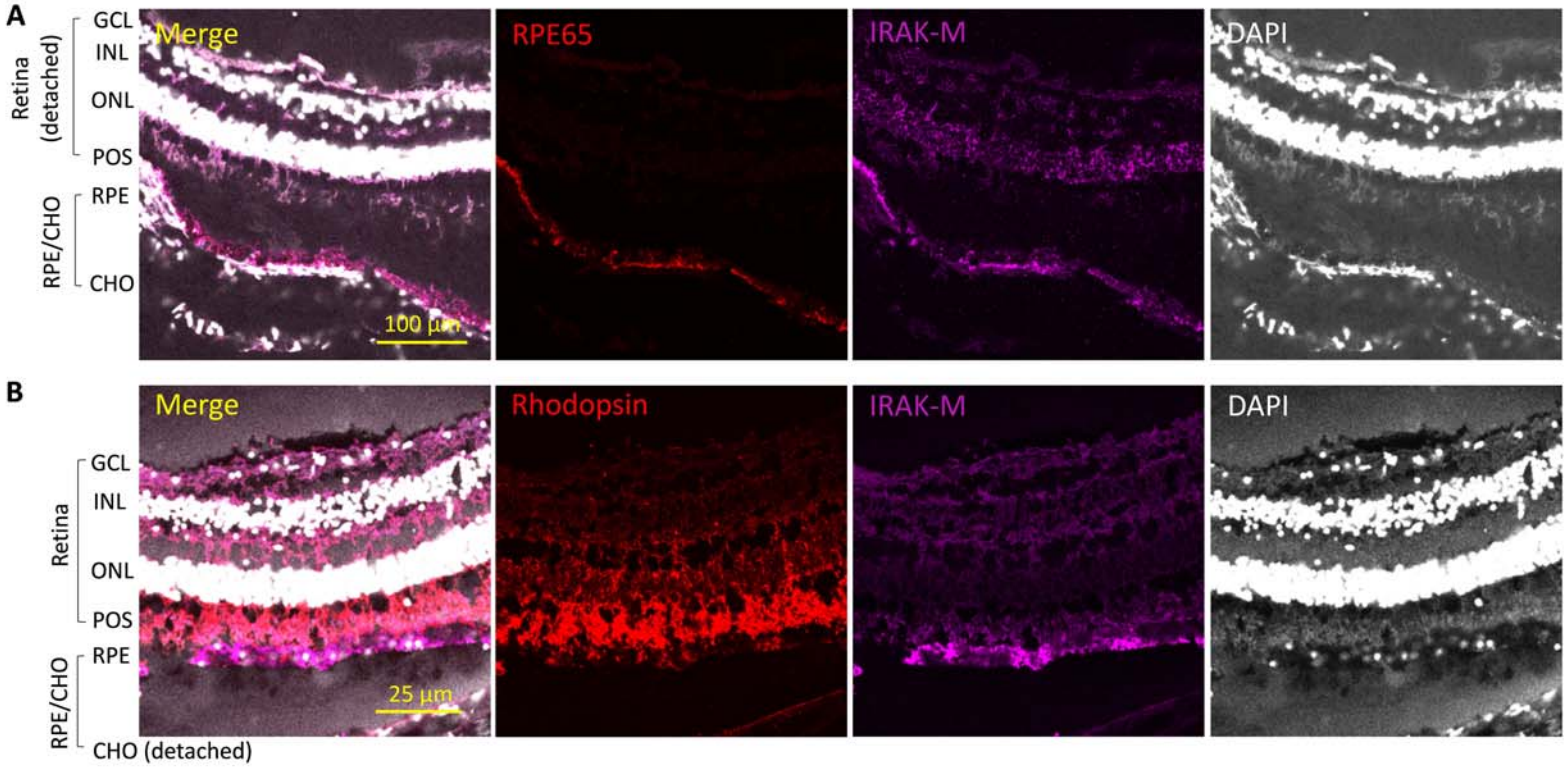
A
Retina (detached)
GCL
INL
ONL
POS
RPE/CHO
RPE
CHO
Merge
RPE65
IRAK-M
DAPI
100 µm
B
Retina
GCL
INL
ONL
POS
RPE/CHO
RPE
CHO (detached)
Merge
Rhodopsin
IRAK-M
DAPI
25 µm

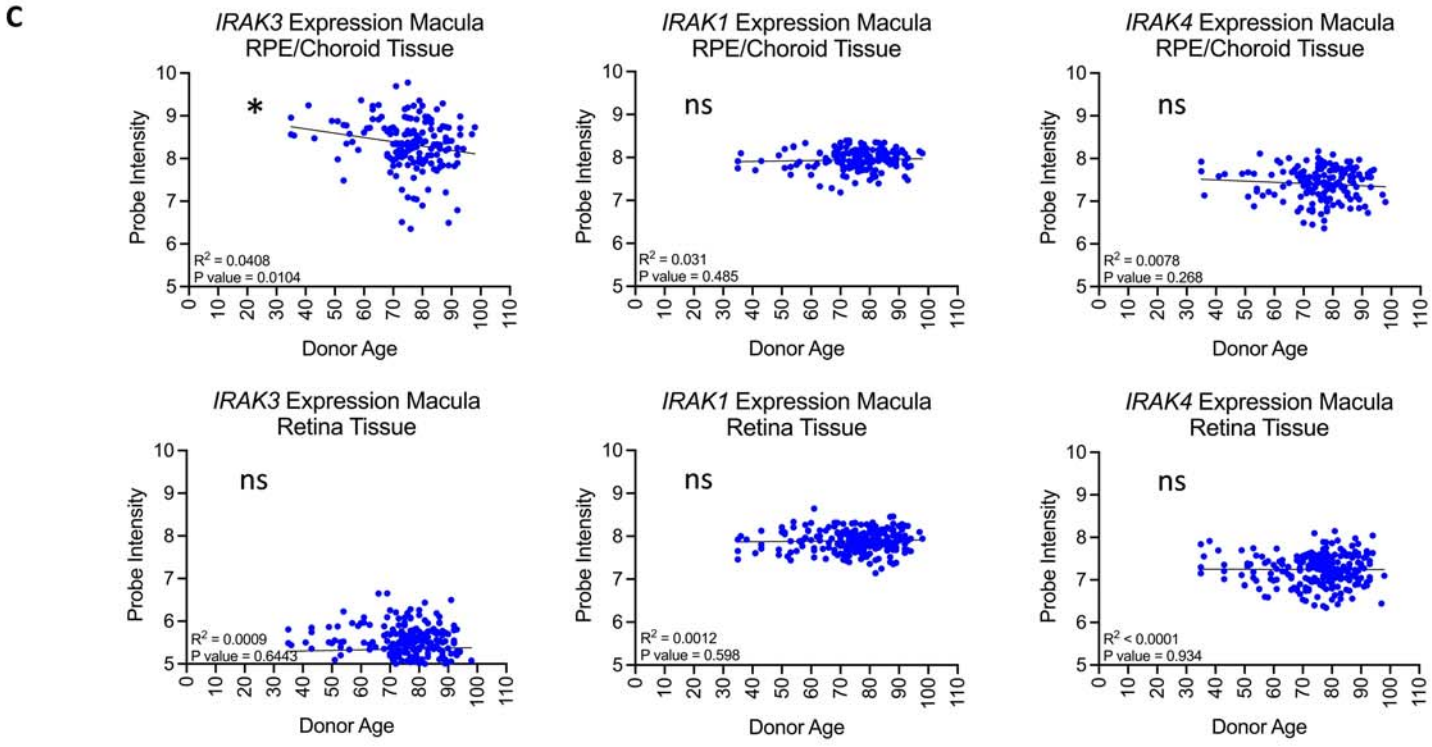
C
IRAK3 Expression Macula RPE/Choroid Tissue
*
R² = 0.0408
P value = 0.0104
IRAK1 Expression Macula RPE/Choroid Tissue
ns
R² = 0.031
P value = 0.485
IRAK4 Expression Macula RPE/Choroid Tissue
ns
R² = 0.0078
P value = 0.268
IRAK3 Expression Macula Retina Tissue
ns
R² = 0.0009
P value = 0.6443
IRAK1 Expression Macula Retina Tissue
ns
R² = 0.0012
P value = 0.598
IRAK4 Expression Macula Retina Tissue
ns
R² < 0.0001
P value = 0.934
Probe Intensity
Donor Age

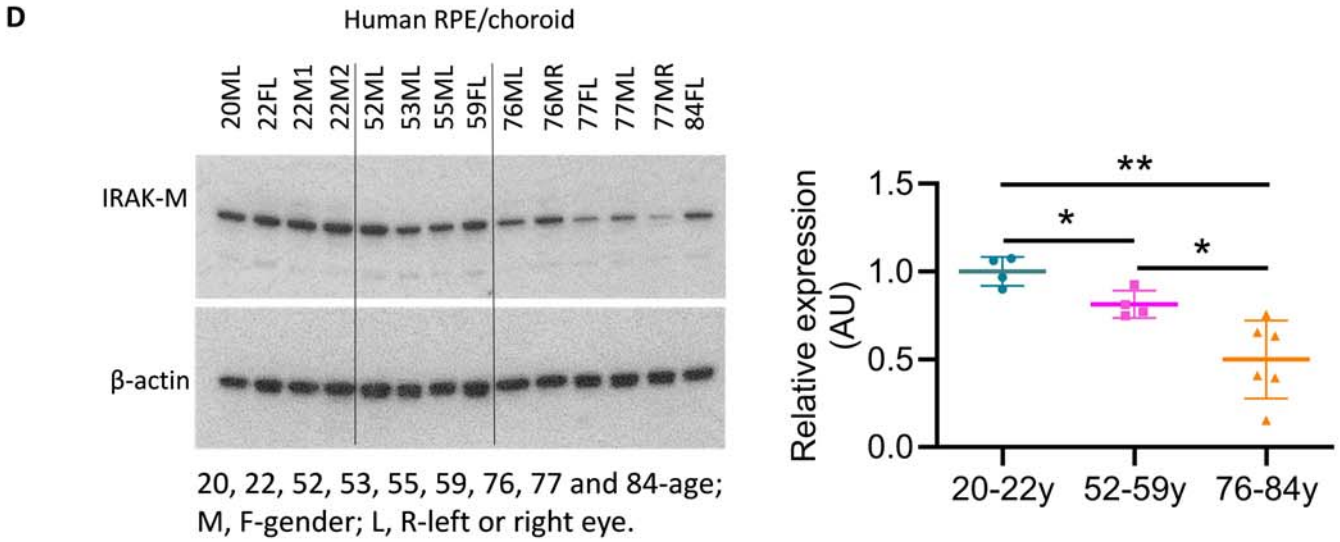
D
Human RPE/choroid
20ML
22FL
22M1
22M2
52ML
53ML
55ML
59FL
76ML
76MR
77FL
77ML
77MR
84FL
IRAK-M
β-actin
20, 22, 52, 53, 55, 59, 76, 77 and 84-age;
M, F-gender; L, R-left or right eye.
Relative expression (AU)
**
*
*
20-22y
52-59y
76-84y

Fig. 2

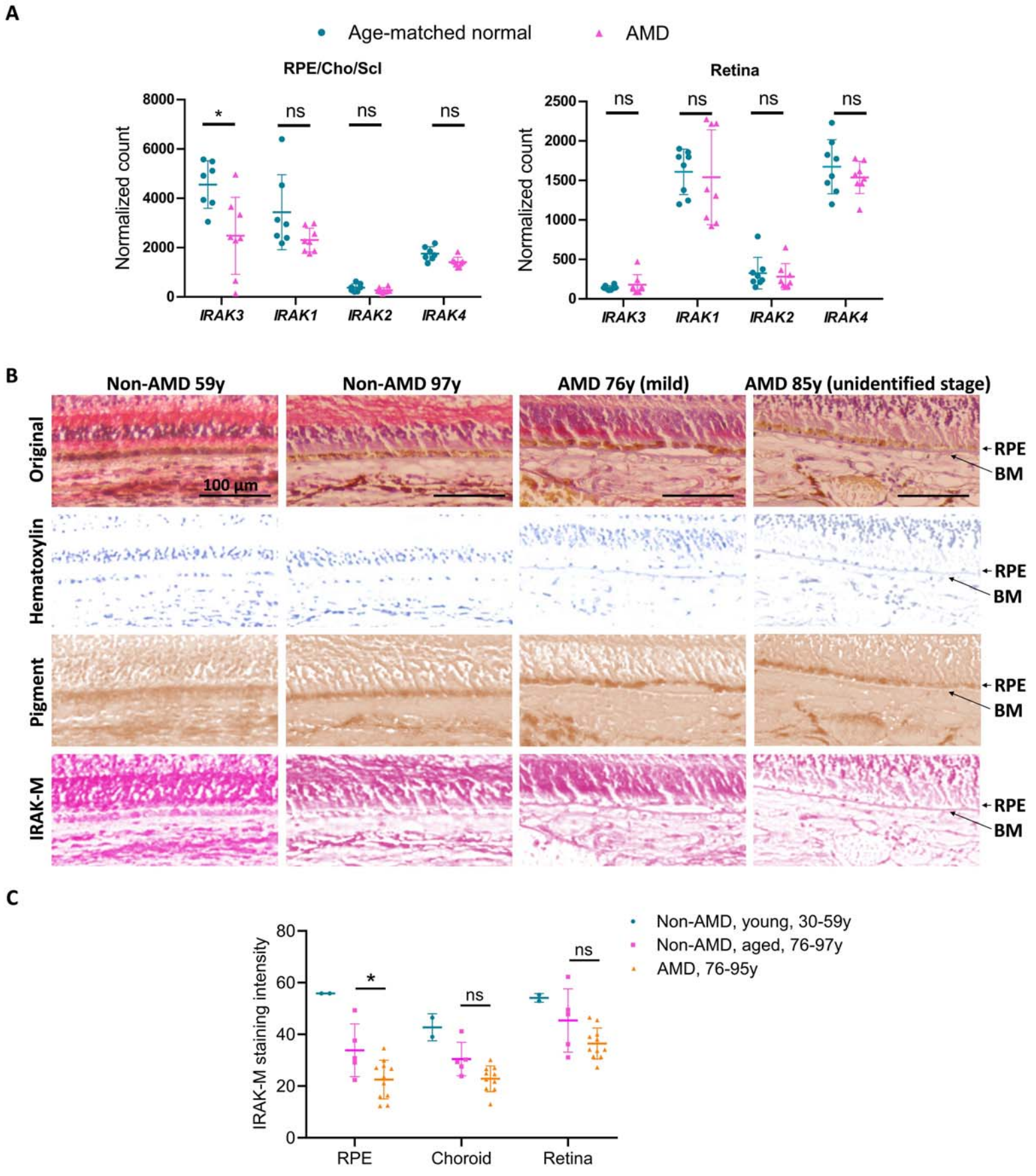
A
Age-matched normal
AMD
RPE/Cho/Scl
Retina
Normalized count
8000
6000
4000
2000
0
2500
2000
1500
1000
500
*
ns
IRAK3
IRAK1
IRAK2
IRAK4
B
Non-AMD 59y
Non-AMD 97y
AMD 76y (mild)
AMD 85y (unidentified stage)
Original
Hematoxylin
Pigment
IRAK-M
100 µm
RPE
BM
C
IRAK-M staining intensity
80
60
40
20
0
RPE
Choroid
Retina
Non-AMD, young, 30-59y
Non-AMD, aged, 76-97y
AMD, 76-95y

Fig. 3

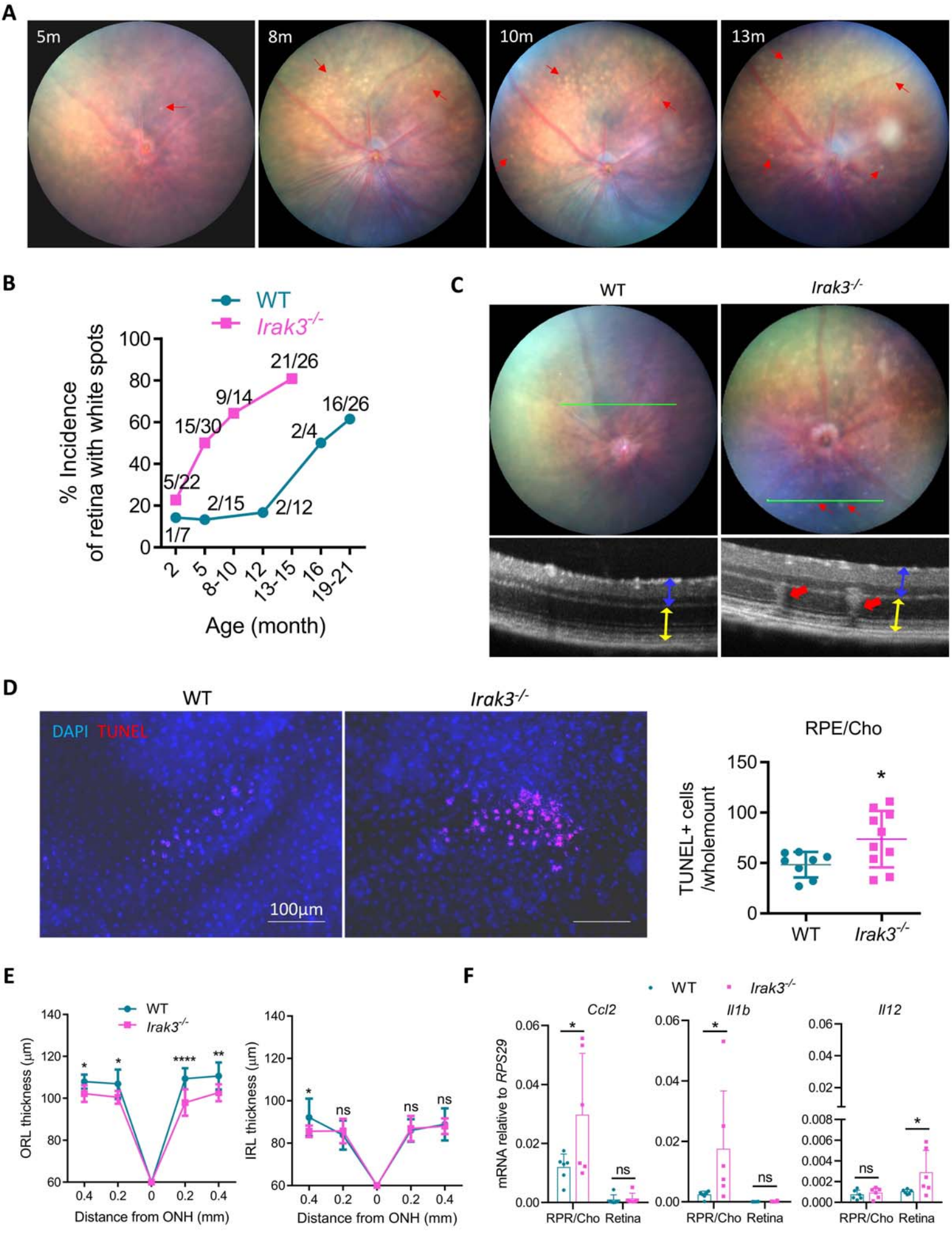
A
5m
8m
10m
13m
B
WT
Irak3-/-
% Incidence of retina with white spots
100
80
60
40
20
0
21/26
9/14
16/26
15/30
2/4
5/22
2/15
2/12
1/7
2
5
8-10
12
13-15
16
19-21
Age (month)
C
WT
Irak3-/-
D
WT
Irak3-/-
DAPI TUNEL
100µm
RPE/Cho
TUNEL+ cells /wholemount
150
100
50
0
*
WT
Irak3-/-
E
WT
Irak3-/-
ORL thickness (µm)
IRL thickness (µm)
140
120
100
80
60
*
*
****
**
ns
ns
ns
0.4
0.2
0
0.2
0.4
Distance from ONH (mm)
F
WT
Irak3-/-
Ccl2
Il1b
Il12
mRNA relative to RPS29
0.06
0.04
0.02
0.008
0.006
0.004
0.002
0.000
0.00
*
ns
RPR/Cho
Retina

Fig. 4

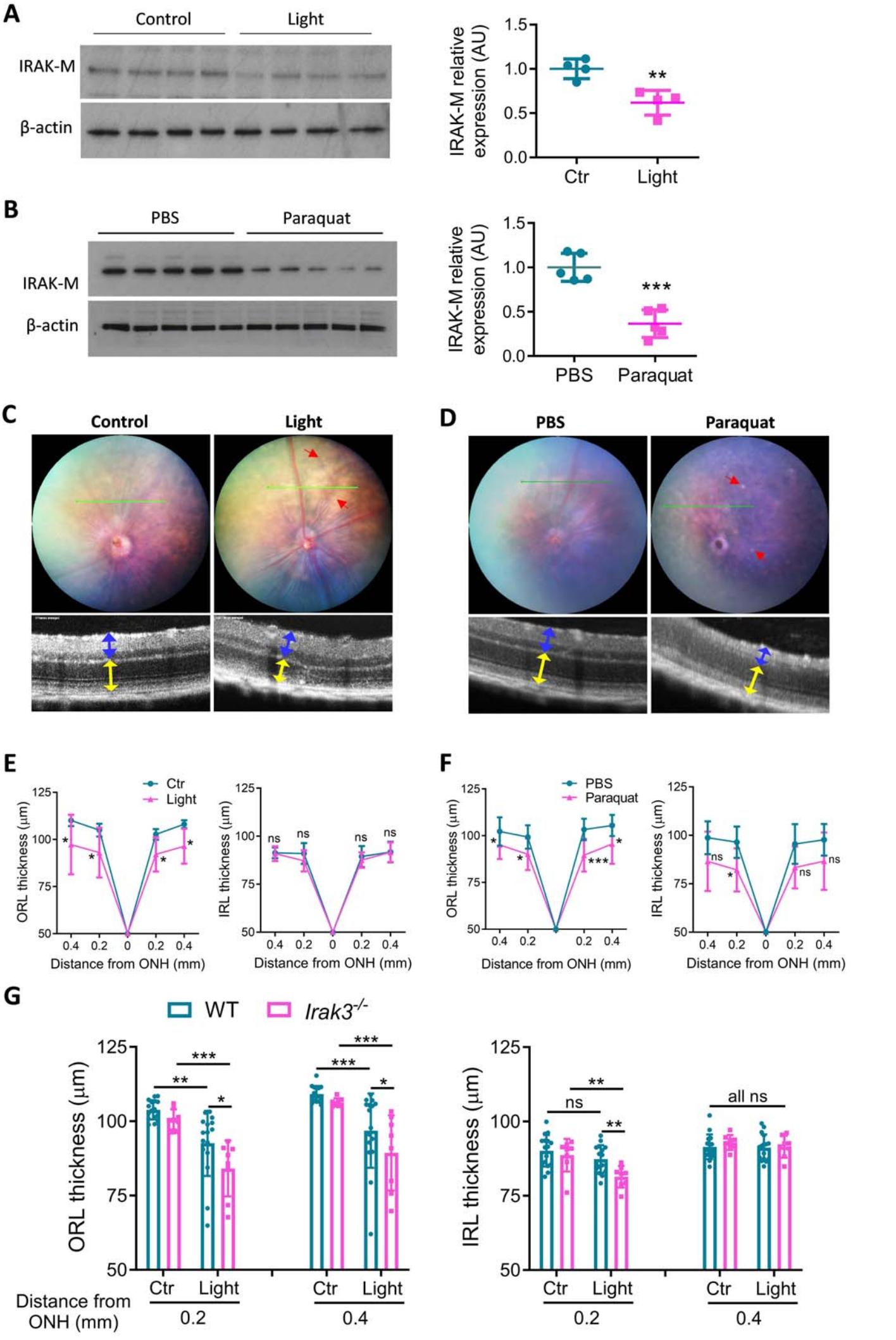
A
Control
Light
IRAK-M
β-actin
IRAK-M relative expression (AU)
1.5
1.0
0.5
0.0
**
Ctr
Light
B
PBS
Paraquat
IRAK-M
β-actin
IRAK-M relative expression (AU)
1.5
1.0
0.5
0.0
***
PBS
Paraquat
C
Control
Light
D
PBS
Paraquat
E
Ctr
Light
ORL thickness (μm)
125
100
75
50
0.4 0.2 0 0.2 0.4
Distance from ONH (mm)
IRL thickness (μm)
ns
F
PBS
Paraquat
ORL thickness (μm)
***
IRL thickness (μm)
G
WT
Irak3-/-
ORL thickness (μm)
IRL thickness (μm)
Distance from ONH (mm)
Ctr
Light
0.2
0.4
ns
all ns

Fig. 5

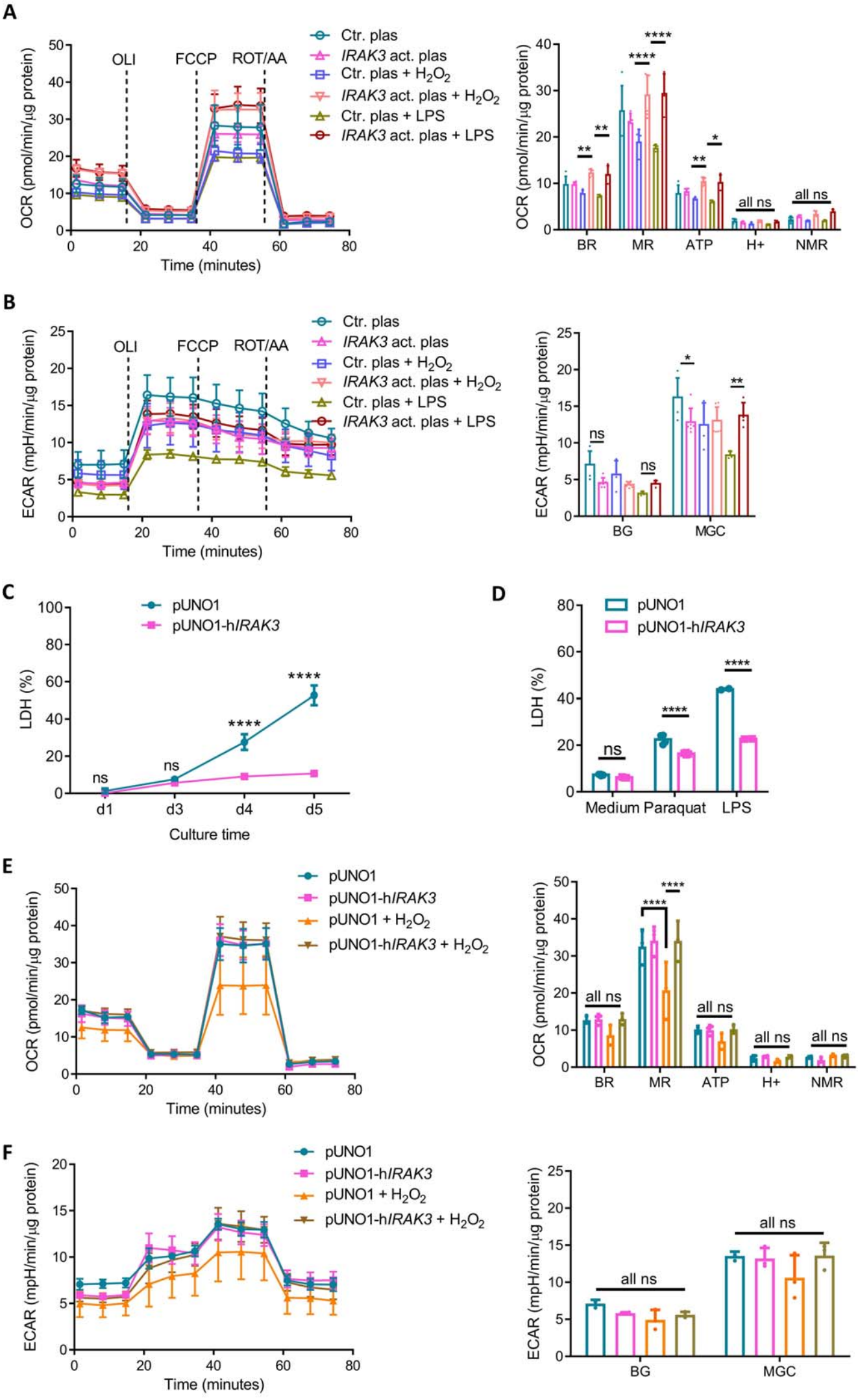
A
OCR (pmol/min/µg protein)
OLI
FCCP
ROT/AA
Time (minutes)
Ctr. plas
IRAK3 act. plas
Ctr. plas + H2O2
IRAK3 act. plas + H2O2
Ctr. plas + LPS
IRAK3 act. plas + LPS
BR
MR
ATP
H+
NMR
all ns
B
ECAR (mpH/min/µg protein)
BG
MGC
C
LDH (%)
pUNO1
pUNO1-hIRAK3
Culture time
d1
d3
d4
d5
D
Medium
Paraquat
LPS
E
pUNO1 + H2O2
pUNO1-hIRAK3 + H2O2
F

Fig. 6

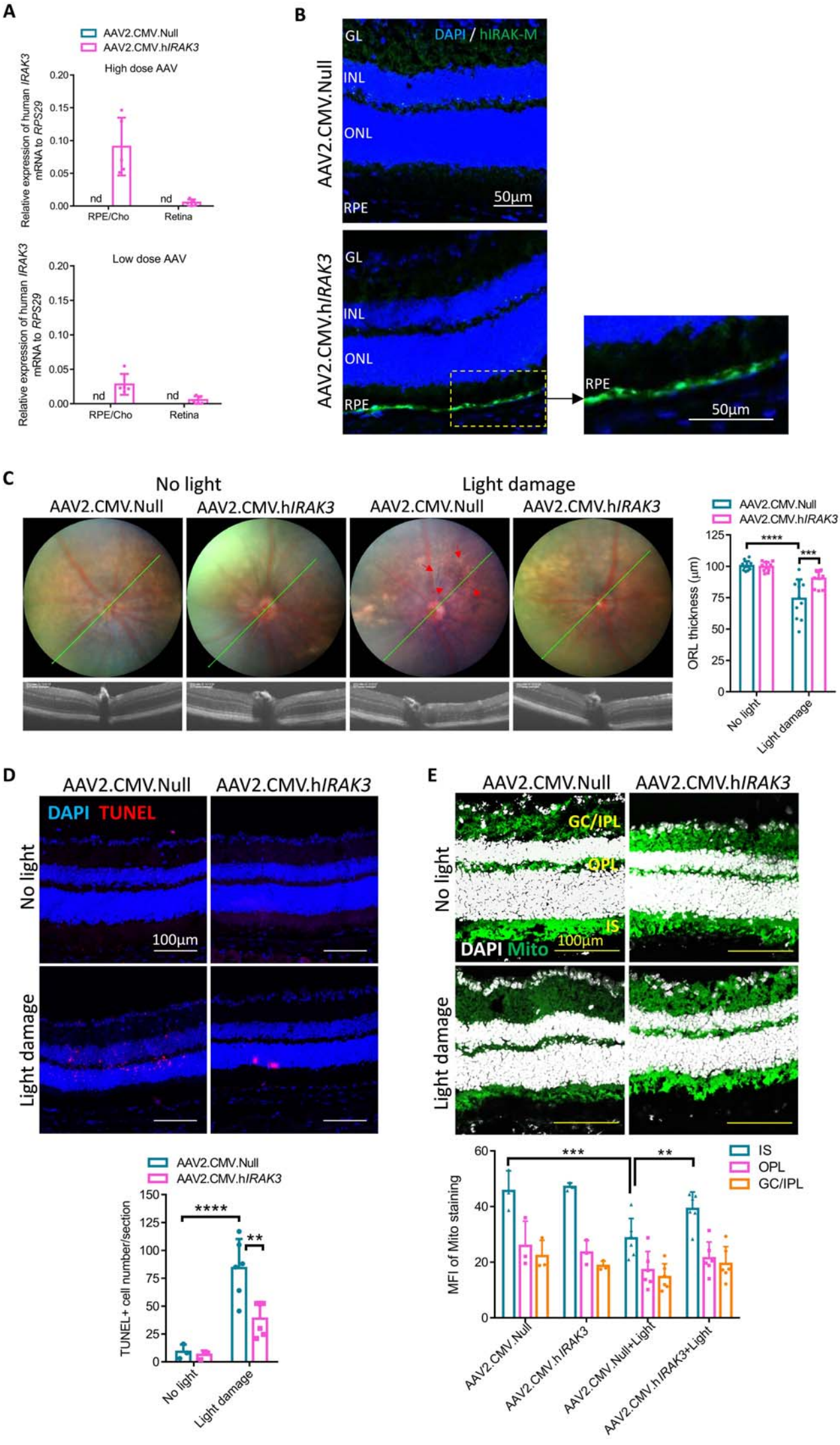
A
AAV2.CMV.Null
AAV2.CMV.hIRAK3
High dose AAV
Relative expression of human IRAK3 mRNA to RPS29
0.20
0.15
0.10
0.05
0.00
nd
nd
RPE/Cho
Retina
Low dose AAV
Relative expression of human IRAK3 mRNA to RPS29
0.20
0.15
0.10
0.05
0.00
nd
nd
RPE/Cho
Retina
B
AAV2.CMV.Null
GL
DAPI / hIRAK-M
INL
ONL
RPE
50μm
AAV2.CMV.hIRAK3
GL
INL
ONL
RPE
RPE
50μm
C
No light
Light damage
AAV2.CMV.Null
AAV2.CMV.hIRAK3
AAV2.CMV.Null
AAV2.CMV.hIRAK3
AAV2.CMV.Null
AAV2.CMV.hIRAK3
ORL thickness (μm)
125
100
75
50
25
0
****
***
No light
Light damage
D
AAV2.CMV.Null
AAV2.CMV.hIRAK3
DAPI TUNEL
No light
100μm
Light damage
AAV2.CMV.Null
AAV2.CMV.hIRAK3
TUNEL+ cell number/section
150
125
100
75
50
25
0
****
**
No light
Light damage
E
AAV2.CMV.Null
AAV2.CMV.hIRAK3
No light
GC/IPL
OPL
IS
DAPI Mito
100μm
Light damage
IS
OPL
GC/IPL
MFI of Mito staining
60
40
20
0
***
**
AAV2.CMV.Null
AAV2.CMV.hIRAK3
AAV2.CMV.Null+Light
AAV2.CMV.hIRAK3+Light

Fig. 7

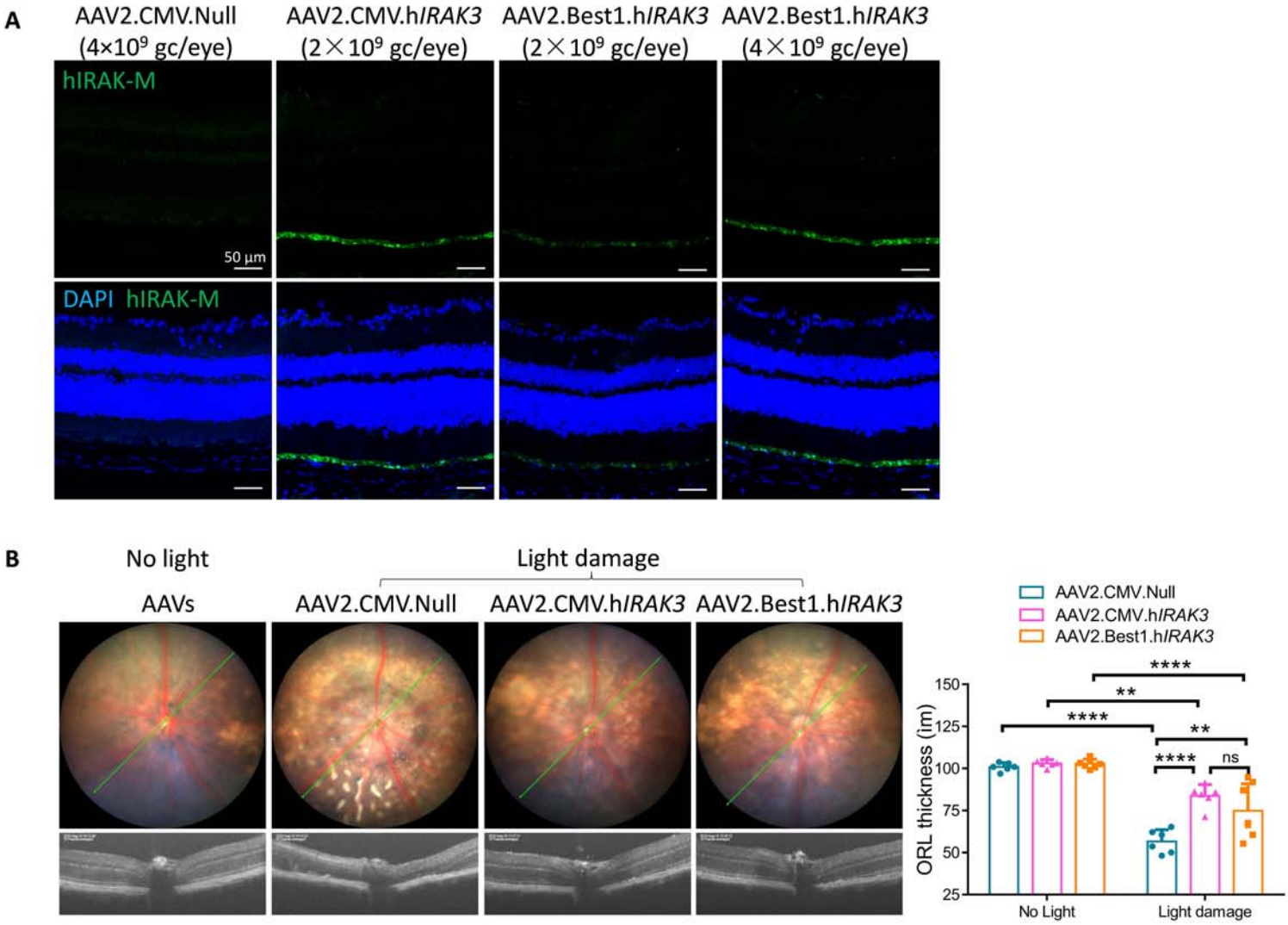
A
AAV2.CMV.Null (4×10^9 gc/eye)
AAV2.CMV.hIRAK3 (2×10^9 gc/eye)
AAV2.Best1.hIRAK3 (2×10^9 gc/eye)
AAV2.Best1.hIRAK3 (4×10^9 gc/eye)
hIRAK-M
50 μm
DAPI hIRAK-M
B
No light
Light damage
AAVs
AAV2.CMV.Null
AAV2.CMV.hIRAK3
AAV2.Best1.hIRAK3
AAV2.CMV.Null
AAV2.CMV.hIRAK3
AAV2.Best1.hIRAK3
ORL thickness (im)
150
125
100
75
50
25
****
**
****
**
****
ns
No Light
Light damage
C
DAPI
ZO-1
Tom20
Merge
No light
AAVs
50 μm
Light damage
AAV2.CMV.Null
AAV2.CMV.hIRAK3
AAV2.Best1.hIRAK3

Fig. 8

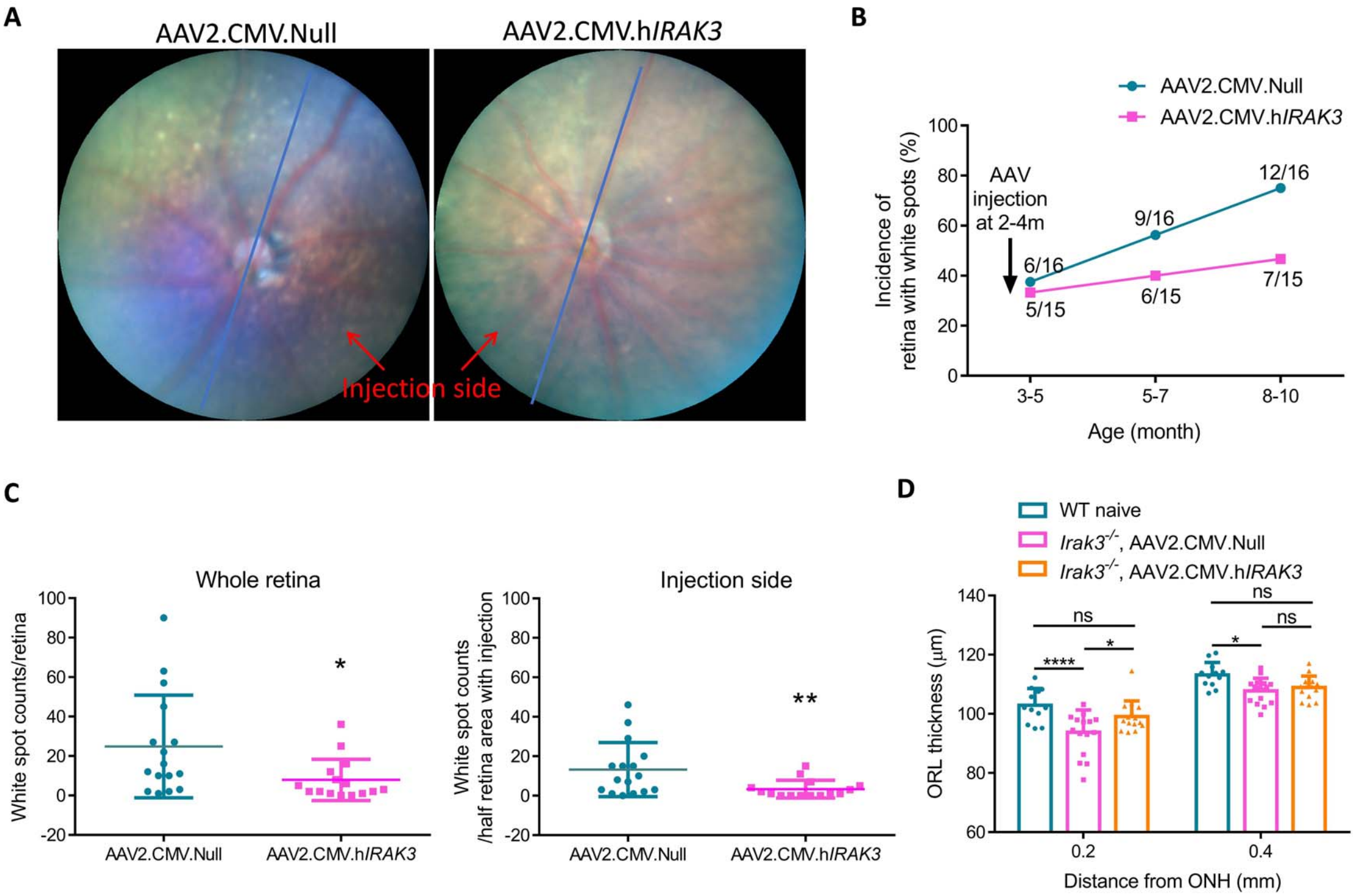
A
AAV2.CMV.Null
AAV2.CMV.hIRAK3
Injection side
B
AAV2.CMV.Null
AAV2.CMV.hIRAK3
Incidence of retina with white spots (%)
AAV injection at 2-4m
6/16
5/15
9/16
6/15
12/16
7/15
Age (month)
3-5
5-7
8-10
C
Whole retina
White spot counts/retina
AAV2.CMV.Null
AAV2.CMV.hIRAK3
Injection side
White spot counts /half retina area with injection
D
WT naive
Irak3-/-, AAV2.CMV.Null
Irak3-/-, AAV2.CMV.hIRAK3
ORL thickness (μm)
Distance from ONH (mm)
ns
****
*
**